Isotropic-nematic phase equilibria in the Onsager theory of hard rods with length polydispersity

Alessandro Speranza and Peter Sollich*
Department of Mathematics, King's College London, Strand, London WC2R 2LS, United Kingdom
(Received 19 December 2002; published 13 June 2003)

We analyze the effect of a continuous spread of particle lengths on the phase behavior of rodlike particles, using the Onsager theory of hard rods. Our aim is to establish whether ''unusual'' effects such as isotropic-nematic-nematic (*I*-*N*-*N*) phase separation can occur even for length distributions with a single peak. We focus on the onset of *I*-*N* coexistence. For a log-normal distribution, we find that a finite upper cutoff on rod lengths is required to make this problem well posed. The cloud curve, which tracks the density at the onset of *I*-*N* coexistence as a function of the width of the length distribution, exhibits a kink; this demonstrates that the phase diagram must contain a three-phase *I*-*N*-*N* region. Theoretical analysis shows that in the limit of large cutoff, the cloud point density actually converges to zero, so that phase separation results at any nonzero density; this conclusion applies to all length distributions with fatter-than-exponentail tails. Finally, we consider the case of a Schulz distribution, with its exponential tail. Surprisingly, even here the long rods (and hence the cutoff) can dominate the phase behavior, and a kink in the cloud curve and *I*-*N*-*N* coexistence again result. Theory establishes that there is a nonzero threshold for the width of the length distribution above which these long-rod effects occur, and shows that the cloud and shadow curves approach nonzero limits for a large cutoff, both in good agreement with the numerical results.

DOI: 10.1103/PhysRevE.67.061702 PACS number(s): 64.70.Md, 05.20.−y, 05.20.Jj, 64.60.−i

I. INTRODUCTION

Rodlike particles such as tobacco mosaic virus in dilute suspension are known to exhibit a phase transition with increasing density between an isotropic phase (*I*) with no orientational or translational order and a nematic phase (*N*) where the rods point, on an average, along a preferred direction [1–5]. The main theoretical approach formulated to predict this phenomenon is the Onsager theory of hard rods [6]. Onsager assumed that the only interaction between the solute particles is of hard core type. The particles are modeled as perfectly rigid, long, thin rods; nonrigidity as well as possible long-range attractive potentials are neglected. Crucially, Onsager showed that the virial expansion truncated after the first nontrivial contribution becomes exact in the limit of long, thin rods (the ''Onsager limit''), i.e., for $D/L_0 \to 0$, where D is the diameter and L_0 the length of the rods. The free energy then assumes a very simple form, because the second virial coefficient is just the excluded volume of two rods. The Onsager limit does however constrain the theory to low densities of the order $\rho \sim O(1/DL_0^2)$, and phases such as smectic phases that occur at higher density cannot be predicted.

In order to express the distribution of the nonconserved rod orientations, Onsager introduced the probability $P(\Omega)$ of finding a rod pointing along the direction Ω. Minimization of the free energy with respect to $P(\Omega)$ results in a self-consistency equation for $P(\Omega)$. Solving this in principle reduces the free energy to a function of density ρ only, so that phase coexistences can be found by a standard double tangent construction. In order to avoid the complexity of the numerical solution [7,8] of the self-consistency equation, Onsager used a simple one-parameter variational trial form for $P(\Omega)$. Using this method Onsager [6] and, two years later Isihara [9], were able to estimate the density at which the *I*-*N* phase transition occurs for different particle shapes. A similar approach was used by Odijk [10], with a Gaussian trial function for $P(\Omega)$. However, the numerically exact solution had by then already been obtained by Kayser and Raveché [11]. An alternative method, based on an expansion of the angular part of the excluded volume in terms of Legendre polynomials [11], was used by Lekkerkerker *et al.* [12]. All of these approaches gave similar results for the properties of the coexisting isotropic and nematic phases.

While being able to solve explicitly only the monodisperse case, Onsager [6] already outlined the possible extension of the theory to *polydisperse* systems, i.e., to mixtures of rods of different lengths and/or different diameters. Polydispersity has indeed been recognized as an important feature affecting experimental results [13,14], and some attempts have been made to include it in theoretical treatments. A generic prediction is the pronounced broadening of the coexistence region with increasing polydispersity [15–18], which is also observed experimentally [14]. A second generic effect of polydispersity is fractionation, i.e., the presence of particles of different sizes in the coexisting phases; for rodlike particles, already Onsager [6] had predicted that the nematic phase would be enriched in the longer rods. Polydispersity can also result in more drastic and qualitative changes to the phase behavior, however. In particular, in systems with length polydispersity coexistence between two nematic phases (*N*-*N*) or one isotropic and two nematic phases (*I*-*N*-*N*) can occur. This has been observed experimentally [13] and predicted theoretically for bi-disperse and tridisperse systems, i.e., mixtures of rods with two or three different lengths [19–23]. However, a detailed investigation of the effects of full length polydispersity, i.e., of a continuous distribution of rod lengths, on the Onsager theory remains an open problem.

*Email address: peter.sollich@kcl.ac.uk

Perturbative approaches [16,17] by their nature cannot access qualitative changes to the phase diagram such as the occurrence of *N*-*N* or *I*-*N*-*N* coexistence. Our lead question for this paper is therefore: can *N*-*N* and *I*-*N*-*N* coexistences occur in length-polydisperse systems of thin hard rods? In cases where the length distribution has two or three pronounced peaks, one expects a behavior similar to the bidisperse or tridisperse case, so that the answer should be positive. Much less clear is what to expect for unimodal length distributions, and this is the case that we will consider.

We concentrate on the onset of isotropic-nematic phase coexistence coming from low density, i.e., on the isotropic cloud point; this can be calculated numerically with some effort using an algorithm that solves directly the integral equation for the orientational distribution of the nematic phase. We choose to start our analysis from a fat-tailed (log-normal) length distribution with a finite upper cutoff on rod length. This choice is inspired by the interesting results obtained by Šolc [24,25] for polydisperse homopolymers, and by our recent investigation [26] of length polydispersity effects within the $\mathcal{P}_2$ Onsager model; the latter is obtained by a simplification of the angular dependence of the excluded volume of the Onsager theory. We showed that within this simplified model *I*-*N*-*N* coexistence is indeed possible in a system with a log-normal (and hence unimodal) rod length distribution. The cloud curve, which gives the density where phase separation first occurs as a function of the width of the length distribution, exhibits a kink where the system switches between two different branches of *I*-*N* phase coexistence. The shadow curve, which similarly records the density of the incipient nematic ''shadow'' phase, has a corresponding discontinuity. Precisely at the kink in the cloud curve a single isotropic coexists with two different nematics, so that this kink forms the beginning of an *I*-*N*-*N* coexistence region. Both the cloud and the shadow curve were found to depend strongly on the rod cutoff length; in the limit of large cutoff, they approach the same limiting form, which is universal for all length distributions with a fatter-than-exponential tail. The nematic shadow phase has rather peculiar properties, being essentially identical to the coexisting isotropic, except for an enrichment in the longest rods; long rods are also the only ones that have significant orientational order.

The above results for the $\mathcal{P}_2$ Onsager model suggest that also in the unapproximated Onsager theory a rod length distribution with a fat tail should have pronounced effects on the phase behavior. We will show numerically that the cloud curve indeed has a kink, and the shadow curve a corresponding discontinuity, demonstrating that the phase diagram contains a region of *I*-*N*-*N* coexistence. In fact, the effects of the fat-tailed length distribution are even stronger than for the $\mathcal{P}_2$ Onsager model, with the nematic shadow phase containing essentially only the very longest rods in the system. The numerical results leave open a number of questions, and we therefore supplement them with a theoretical analysis. We show that the assumption of a nematic shadow phase dominated by the longest rods is self-consistent, and are able to predict that in the limit of large cutoff the density of the cloud point actually tends to zero: even though the average rod length is finite, the presence of a tail of long rods drives the system to phase separate at any nonzero density. Motivated by these results, we finally revisit the case of rod length distributions with an exponential tail, using the Schulz distribution as an example. Numerical results show, surprisingly, that even here a regime occurs where the cutoff length matters and the nematic shadow phase contains predominantly the longest rods; a kink in the cloud curve again reveals the presence of an *I*-*N*-*N* coexistence region. (This is in stark contrast to our results for the $\mathcal{P}_2$ Onsager model [27], where the exponential tail of the distribution produces no unusual effects.) By returning to our theoretical analysis, we find that the long-rod effects are weaker for the Schulz distribution than for the log-normal case: they only occur above a certain threshold value for the width of the rod length distribution, and the large-cutoff limits of the cloud and shadow densities above this threshold remain nonzero.

The paper is structured as follows. In Sec. II, we outline the extension to continuous length distributions of the Onsager theory and derive the phase coexistence equations for the isotropic cloud point. Section III describes the numerical method used to locate the cloud point and gives our results for the phase behavior for log-normal length distributions with finite cutoff. In Sec. IV, we outline our theory for the large-cutoff limit and compare with numerical results at finite but large cutoff. Finally, in Sec. V we turn to systems with a Schulz distribution of lengths, giving numerical results and sketching an appropriately modified theoretical analysis. Section VI contains a summary and a discussion of avenues for future work. In Appendix A, we review in outline the high-density scaling theory for the monodisperse Onsager theory, which we need in our analysis of the large-cutoff limit. In Appendix B, the main approximation underlying our theory for the log-normal distribution is justified, while the appropriate modifications for the Schulz distribution are sketched in Appendix C.

II. THE POLYDISPERSE ONSAGER THEORY

The Onsager theory with length polydispersity models a system of hard spherocylinders with equal diameters D, but different lengths L. We introduce a reference length scale L_0 and write $L=lL_0$, where l is a dimensionless normalized length. The Onsager limit is then taken by considering $D/L_0 \to 0$ at constant values for the normalized lengths l. From now on, we will refer to l itself as the rod length, unless stated otherwise; it can, in principle, range over all the values between 0 and ∞.

The thermodynamic state of the system is described by the *density distribution* $\rho(l,\Omega)$. This is defined such that $\rho(l,\Omega)\, dl\, (d\Omega/4\pi)$ is the number density of rods with lengths in the range $l \ldots l+dl$ and pointing along a direction within the solid angle $d\Omega$ around Ω. In terms of spherical coordinates, with the z direction taken to be the nematic axis, we have $d\Omega = \sin\theta\, d\theta\, d\varphi$ and the density distribution is independent of the azimuthal angle φ, $\rho(l,\Omega) \equiv \rho(l,\theta)$. It can thus be decomposed according to

$$\rho(l,\theta) = \rho(l) P(\theta|l) = \rho P(l) P(\theta|l).$$

Here, $\rho(l)$ is the density distribution over lengths,

$$\rho(l)=\int \frac{d\Omega}{4\pi}\ \rho(l,\theta)=\frac{1}{2}\int d\cos\theta\ \rho(l,\theta)=\int \widetilde{d\theta}\ \rho(l,\theta),$$

where we have introduced the shorthand

$$\widetilde{d\theta}=\frac{1}{2}d\cos\theta.$$

The overall rod number density is

$$\rho=\int dl\,\rho(l)=\int dl\,\widetilde{d\theta}\,\rho(l,\theta),$$

so that $P(l)=\rho(l)/\rho$ gives the normalized length distribution. From the definition of $\rho(l)$ it also follows that the orientational distributions $P(\theta|l)$ for rods of fixed length are normalized in the obvious way, $\int\widetilde{d\theta}P(\theta|l)=1$. Notice that the factor 4π in the definition of $\rho(l,\Omega)$ has been chosen so that for an isotropic phase one has the simple expressions $P(\theta|l)=1$ and $\rho(l)=\rho(l,\theta)$.

We can now state the free-energy density for the polydisperse Onsager theory (see, e.g., Ref. [17]). We use units such that $k_BT=1$ and make all densities dimensionless by multiplying with the unit volume $V_0=(\pi/4)DL_0^2$. The free-energy density is then

$$f=\int dl\ \rho(l)[\ln\rho(l)-1]+\int dl\,\widetilde{d\theta}\ \rho(l)P(\theta|l)\ln P(\theta|l)+\frac{1}{2}\int dl\ dl'\widetilde{d\theta}\,\widetilde{d\theta'}\rho(l)\rho(l')P(\theta|l)P(\theta'|l')ll'K(\theta,\theta'). \tag{1}$$

The first term gives the entropy of an ideal mixture, while the second term represents the orientational entropy of the rods. The third term is the appropriate average of the excluded volume $(8/\pi)V_0ll'|\sin\gamma|$ (with V_0 absorbed by our density scaling) of the two rods at an angle γ with each other. The kernel [6,11] $K(\theta,\theta')$ results from the average of $(8/\pi)|\sin\gamma|$ over the azimuthal angles φ,φ' of the rods,

$$K(\theta,\theta')=\frac{8}{\pi}\int_0^{2\pi}\frac{d\varphi'}{2\pi}\frac{d\varphi}{2\pi}|\sin\gamma|=\frac{8}{\pi}\int_0^{2\pi}\frac{d\varphi}{2\pi}\sqrt{1-(\cos\theta\cos\theta'+\sin\theta\sin\theta'\cos\varphi)^2}.$$

As in the monodisperse case, the orientational distributions $P(\theta|l)$ are obtained by minimization of the free energy, Eq. (1); inserting Lagrange multipliers to enforce the normalization of $P(\theta|l)$, one finds

$$P(\theta|l)=\frac{e^{l\psi(\theta)}}{\int\widetilde{d\theta'}e^{l\psi(\theta')}}, \tag{2}$$

$$\psi(\theta)=-\int dl'\widetilde{d\theta'}\rho(l')P(\theta'|l')l'K(\theta,\theta'). \tag{3}$$

The conditions for phase equilibrium are that the coexisting phases must have equal chemical potential $\mu(l)$ for all rod lengths l, as well as equal osmotic pressure. The chemical potentials can be obtained by functional differentiation of the free energy (1) with respect to $\rho(l)$. The orientational distributions $P(\theta|l)$ do depend on $\rho(l)$ but this dependence can be ignored because f, having been minimized, is stationary with respect to the $P(\theta|l)$. Carrying out the differentiation and inserting Eq. (2) gives

$$\mu(l)=\frac{\delta f}{\delta\rho(l)}=\ln\rho(l)+\int\widetilde{d\theta}\ P(\theta|l)\left[l\psi(\theta)-\ln\int\widetilde{d\theta'}e^{l\psi(\theta')}\right]+\int dl'\widetilde{d\theta}\,\widetilde{d\theta'}\rho(l')P(\theta|l)P(\theta'|l')ll'K(\theta,\theta') \tag{4}$$

$$=\ln\rho(l)-\ln\int\widetilde{d\theta}\ e^{l\psi(\theta)}. \tag{5}$$

The osmotic pressure can be obtained from the Gibbs-Duhem relation, which for a polydisperse system reads

$$\Pi=\int dl\,\mu(l)\rho(l)-f.$$

Inserting Eqs. (2) and (4) then yields

$$\Pi=\rho-\frac{1}{2}\int dl\,\widetilde{d\theta}\ l\rho(l)P(\theta|l)\psi(\theta). \tag{6}$$

A. Isotropic-nematic phase coexistence

We now specialize the phase coexistence conditions to *I-N* coexistence, and then eventually to the isotropic cloud point, i.e., the onset of *I-N* coexistence coming from low densities. The isotropic phase will have

$$P^I(\theta|l)=1,\quad \psi^I(\theta)=\psi^I=-c_1\rho_1^I,\quad \Pi^I=\rho^I+\frac{1}{2}c_1(\rho_1^I)^2, \tag{7}$$

where we have defined the first moment ρ_1 of the density distribution $\rho(l,\theta)$,

$$\rho_1=\int dl\,l\rho(l)=\rho\int dl\,lP(l)=\rho\langle l\rangle,$$

which represents the scaled rod volume fraction $\rho_1=(L_0/D)\phi$. We have also used the fact that the average of the kernel $K(\theta,\theta')$ over one of its arguments is just an isotropic average over $(8/\pi)|\sin\gamma|$, giving

$$\int \widetilde{d\theta'} K(\theta,\theta') = \frac{8}{\pi}\frac{1}{2}\int_0^\pi d\gamma \sin\gamma|\sin\gamma| = \frac{8}{\pi}\frac{\pi}{4} = 2 \equiv c_1 .$$

The equality of the chemical potentials (5) gives for the density distribution in the nematic phase,

$$\rho^N(l) = \rho^I(l) \int \widetilde{d\theta}\, e^{lg(\theta)}, \tag{8}$$

where

$$g(\theta) = \psi^N(\theta) - \psi^I = \psi^N(\theta) + c_1\rho_1^I . \tag{9}$$

The full density distribution over lengths and orientations is therefore, using Eq. (2),

$$\rho^N(l,\theta) = \rho^N(l) P^N(\theta|l) = \rho^I(l) e^{lg(\theta)} \tag{10}$$

and the osmotic pressure (6) of the nematic phase can be rewritten as

$$\Pi^N = \int dl\, \widetilde{d\theta}\, \rho^I(l) e^{lg(\theta)} - \frac{1}{2}\int dl\, \widetilde{d\theta} l\, \rho^I(l) e^{lg(\theta)} \psi^N(\theta). \tag{11}$$

In the following, we will concentrate on the isotropic cloud point, where the isotropic ''cloud'' phase starts to coexist with an infinitesimal amount of nematic ''shadow'' phase. At the cloud point, the isotropic density distribution over lengths, $\rho^I(l)$, therefore coincides with the overall density distribution of the system, $\rho^{(0)}(l)$, which we call the *parent distribution*. It can be written as $\rho^{(0)}(l) = \rho P^{(0)}(l)$, where $\rho = \int dl\, \rho^{(0)}(l)$ is the overall parent number density and $P^{(0)}(l)$ the normalized parent length distribution. Since all properties of the isotropic cloud phase are determined by the parent, we will drop the superscript ''I'' in the following. We will also take the parent distribution to have an average length $\langle l\rangle = 1$; any other choice could be absorbed into the reference length L_0. This implies that the density and (scaled) volume fraction of the isotropic phase are equal, $\rho_1 = \rho$. With this notation, the density distribution (10) of the nematic shadow is $\rho^N(l,\theta) = \rho P^{(0)}(l) e^{lg(\theta)}$ and fully determined by ρ and $g(\theta)$. The function $g(\theta)$ must obey

$$g(\theta) = -\rho \int dl\, \widetilde{d\theta'}\, P^{(0)}(l) e^{lg(\theta')} l K(\theta,\theta') + c_1\rho \tag{12}$$

as follows from Eq. (3) for $\psi^N(\theta)$ together with Eq. (9). The cloud point density is the smallest value of ρ for which in addition the pressure equality is satisfied. Using Eq. (7) for the pressure of the isotropic, and Eqs. (9) and (11) for that of the nematic, this condition reads

$$\rho + \frac{1}{2}c_1\rho^2 = \rho \int dl\, \widetilde{d\theta}\, P^{(0)}(l) e^{lg(\theta)} - \frac{\rho}{2}\int dl\, \widetilde{d\theta}\, l P^{(0)}(l) e^{lg(\theta)} [g(\theta) - c_1\rho]. \tag{13}$$

B. Fat-tailed rod length distributions

So far, everything is general and applies to any parent length distribution $P^{(0)}(l)$. Let us now focus on the case of a parent distribution with a fat, i.e., less than exponentially decaying tail for large l. At the cloud point we have from Eq. (8) the density distribution $\rho^N(l) = \rho P^{(0)}(l) \int \widetilde{d\theta}\, e^{lg(\theta)}$ in the nematic shadow phase, or if we isolate the value of $g(\theta)$ at $\theta = 0$

$$\rho^{\mathrm{N}}(l) = \rho P^{(0)}(l) e^{lg(0)} \int \widetilde{d\theta}\, e^{l[g(\theta) - g(0)]}. \tag{14}$$

In a nematic phase, one expects $g(\theta) \leqslant g(0)$ and therefore the angular integral reduces to a less than exponentially varying function of l. Moreover, $g(0)$ is expected to be positive, since the nematic phase should contain the longer rods. The nematic density distribution $\rho^N(l)$ is therefore exponentially diverging for large l whenever the normalized parent distribution $P^{(0)}(l)$ decays less than exponentially. In order to ensure finite values for the density and volume fraction of the nematic phase, we thus need to impose a finite cutoff l_m on the length distribution; unless otherwise specified, all l integrals will therefore run over $0 \ldots l_m$ from now on. The presence of a cutoff is of course also physically reasonable, since any real system contains a finite largest rod length. Nevertheless, we will later also consider the limit of infinite cutoff, which highlights the effects of the presence of long rods.

III. NUMERICAL RESULTS FOR THE ONSET OF *I-N* COEXISTENCE

A. Numerical method

A numerical determination of the isotropic cloud point involves the solution of the two coupled equations (12) and (13) for ρ and $g(\theta)$. In an outer loop we vary the density until the smallest ρ that satisfies the pressure equality (13) is found; we use a false position method [28]. The nontrivial part of the algorithm is the inner loop, i.e., the solution of the functional equation (12) for $g(\theta)$ at given ρ. An iterative method inspired by the one used by Herzfeld *et al.* [7] for the monodisperse case turns out to converge too slowly in the presence of polydispersity. We therefore choose to represent $g(\theta)$ by its values $g_i = g(\theta_i)$ at a set of n discrete points θ_i; the values of $g(\theta)$ for $\theta \neq \theta_i$ are then assumed to be given by a cubic spline fit [29] through the points (θ_i, g_i). This turns the functional equation (12) into a set of n nonlinear coupled equations which can be solved by, e.g., a Newton-Raphson algorithm [28]. To keep n manageably small while keeping the spline representation accurate, a judicious choice of θ_i is important. We exploit the symmetry $g(\theta) = g(\pi - \theta)$ and choose a nonlinear (geometric) spacing of θ_i over the range $0 \ldots \pi/2$, with more points around the origin, where $g(\theta)$ is least smooth.

While Eqs. (12) and (13), in principle, involve double integrals over θ and l, one notices that only the two l integrals

$$h(x)=\int dl\ P^{(0)}(l)e^{lx},\quad h'(x)=\int dl\ P^{(0)}(l)\,le^{lx}$$

are needed. We therefore precompute these and store them once and for all as cubic spline fits that can be evaluated very efficiently.

As an alternative to the approach above, we also considered calculating $g(\theta)$ by minimizing an appropriate functional. If $\mu^I(l)$ and Π^I are the chemical potentials and osmotic pressure of the isotropic parent phase, then one easily sees that a local minimum of the functional

$$\Xi[\rho(l,\theta)]=f[\rho(l,\theta)]-\int dl\ \widetilde{d\theta}\ \mu^I(l)\rho(l,\theta)+\Pi^I \tag{15}$$

corresponds to a phase $\rho(l,\theta)$ with the same chemical potentials as the parent. Inserting for $\rho(l,\theta)$ the known form (10) for the nematic density distribution, Ξ turns into a functional of $g(\theta)$, and the condition for a local minimum becomes equivalent to Eq. (12). $\Xi[g(\theta)]$ always has $g(\theta)\equiv 0$ as a minimum, corresponding to the isotropic parent itself; but close to the onset of phase coexistence an additional nematic solution with $g(\theta)\neq 0$ appears. Notice that, geometrically, Ξ is a tilted version of the free energy for which the tangent (hyper)plane at the parent is horizontal ($\Xi=0$). At phase coexistence, i.e., for a parent with the cloud point density, the tangent plane also touches the nematic phase and so the isotropic and the nematic minima of Ξ are both at "height" $\Xi=0$.

Numerically, one could minimize Ξ by again representing $g(\theta)$ as a spline through a finite number of points $g_i=g(\theta_i)$ and then minimizing the resulting function of the g_i. In general, this turns out to be no easier than the solution of the similarly discretized version of Eq. (12). However, the minimization approach *is* useful when $g(\theta)$ assumes a simple parametric form. We will see later that this is indeed the case for a large cutoff l_m, with $g(\theta)$ being well approximated by the two-parameter form $g(\theta)=a-b\sin\theta$. Inserting this into Ξ and minimizing over a and b then gives an approximate solution for $g(\theta)$; when used as a starting point for $g(\theta)$, this makes it significantly easier to converge the numerical solution of the discretized equation (12) described above.

B. Results for log-normal length distribution

With the numerical method described in the preceding section, it is possible to solve for the onset of isotropic-nematic phase coexistence for, in principle, arbitrary parent length distribution. We choose here a specific fat-tailed length distribution, the log-normal, that has already given interesting results in polymers [24] and in our previous analysis of the $\mathcal{P}_2$ Onsager model [26]. The log-normal distribution has the form

$$P^{(0)}(l)=\frac{1}{\sqrt{2\pi w^2}}\frac{1}{l}\exp\left[-\frac{(\ln l-\mu)^2}{2w^2}\right] \tag{16}$$

with a finite length cutoff l_m. The quantity w, which tunes the width of the distribution, is fixed by the normalized standard deviation σ (in the following referred to as polydispersity),

$$\sigma^2=\frac{\langle l^2\rangle-\langle l\rangle^2}{\langle l\rangle^2}$$

to be $w^2=\ln(1+\sigma^2)$. The second parameter μ is determined so that the parent has average length $\langle l\rangle=1$, giving $\mu=-w/2$. Notice that with these choices, the parent length distribution is normalized and has the desired moments $\langle l\rangle=1$ and $\langle l^2\rangle=1+\sigma^2$ only in the limit of infinite cutoff l_m. The deviations for finite cutoffs are small even for relatively modest l_m, however. For instance, at cutoff $l_m=50$ and $\sigma=0.5$, the integrals $\int_0^{l_m}dl\ l^nP^{(0)}(l)$ for $n=0,1,2$ differ from their respective values at infinite cutoff (1, 1, and 1.25) by values of order 10^{-17}, 10^{-15}, and 10^{-13}. Since we will not consider smaller cutoff values below, these small corrections can safely be neglected.

In our previous analysis of the $\mathcal{P}_2$ Onsager model [26], we observed that for log-normal length distributions, the cloud curve has a kink, and the shadow curve a corresponding discontinuity; at the kink, the isotropic phase is in coexistence with two distinct nematics, so that the phase diagram must contain a region of *I-N-N* coexistence. In the $\mathcal{P}_2$ Onsager case, the simplicity of the model actually allowed us to compute the complete phase diagram and locate the three-phase *I-N-N* region explicitly. For the full Onsager theory treated here, we can only find the cloud and shadow curves at present, not the full phase diagram; nevertheless, a kink in the cloud curve will again imply the presence of an *I-N-N* region in the full phase diagram. In Fig. 1, we show the cloud and shadow curves, i.e., the number density of the isotropic cloud (a) and nematic shadow (b) plotted against polydispersity, for a log-normal parent with two different cutoffs. The presence of the kink in the cloud curves, and the corresponding discontinuity in the shadow curves, is clear evidence of the presence of an *I-N-N* coexistence region starting at the kink of the cloud curve. The positions of the kink and discontinuity, respectively, as well as the shapes of the cloud and shadow curves above them, show a strong dependence on the cutoff length; both curves move to significantly smaller densities as l_m increases. For polydispersities σ below the kink, on the other hand, the number of long rods is too small to have a significant effect on the phase separation and one has essentially cutoff-independent behavior that connects smoothly with the monodisperse limit $\sigma=0$. These observations are in qualitative accord with our earlier results for the $\mathcal{P}_2$ Onsager model with the same length distribution [26].

Moving across the discontinuity from below, the shadow curve jumps from a "normal" nematic branch to an unusual nematic phase which, as we will see below, is completely dominated by the longest rods in the parent distribution. In the rescaled volume fraction (ρ_1) representation of the shadow curve shown in Fig. 2, the different characteristics of the two nematic phases are clear. While at low polydisper-

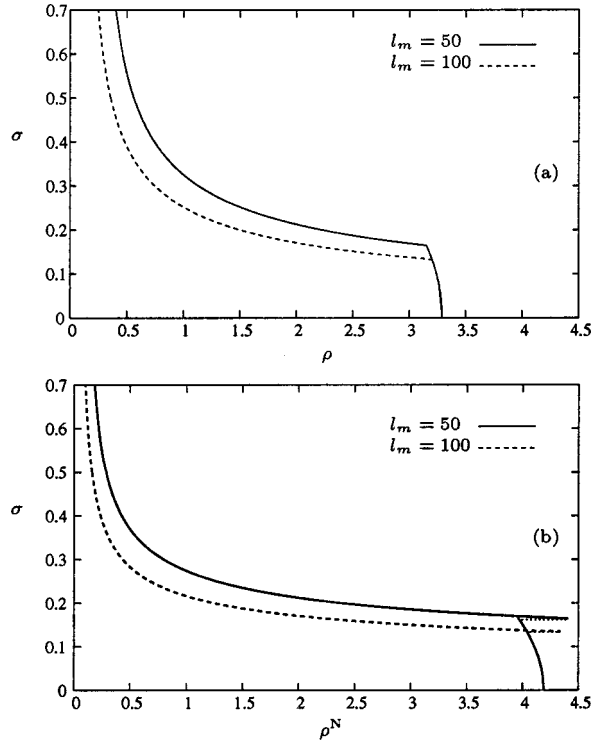

FIG. 1. (a) Number density ρ of the cloud phase for length cutoff $l_m=50$ (solid) and $l_m=100$ (dashed), plotted against the polydispersity σ on the y axis. Notice the kinks in the two curves, which imply the presence of a three-phase I-N-N coexistence region in the full phase diagram. The kinks correspond, as they should, to discontinuities in the shadow curves (b). Both cloud and shadow curves are strongly cutoff dependent, moving towards lower densities as l_m increases.

sity, ρ_1^N is of the order of unity, it jumps by two orders of magnitude on crossing the discontinuity. This shows that the fractionation effect that one normally encounters in polydisperse systems, with the long rods found preferentially in the nematic phase, becomes extreme here. A plot of the average rod length in the nematic shadow against polydispersity (Fig. 3), in fact, shows that above the discontinuity, the nematic phase contains almost exclusively rods of length close to the

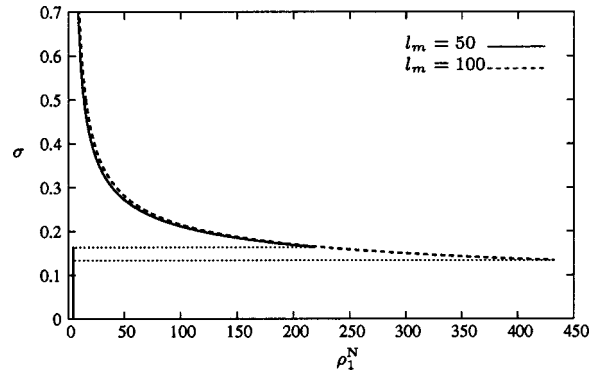

FIG. 2. Scaled volume fraction ρ_1^N of the nematic shadow phase at $l_m=50$ (solid) and $l_m=100$ (dashed). Notice that the discontinuity of the two curves is now much wider than in the number density representation of the shadow curves in Fig. 1(b).

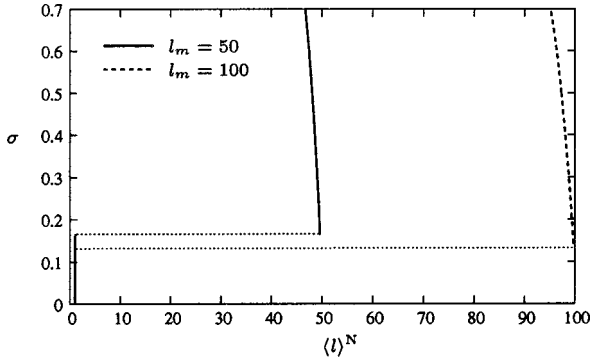

FIG. 3. Average length $\langle l\rangle^N=\rho_1^N/\rho^N$ in the nematic shadow phase against polydispersity for cutoffs $l_m=50$ (solid) and $l_m=100$ (dashed). Above the discontinuity, fractionation becomes extreme. In fact, at the discontinuity the nematic phase appears to be composed only of rods with lengths of the order of the cutoff length. At the top of the plot, for very large polydispersities where the parent length distribution becomes somewhat more uniform, some shorter rods are also included in the nematic phase and reduce the average length.

cutoff length. Since the longer rods are generically expected to be more strongly ordered, one should then also find that the nematic shadow phase has a very strong orientational order. This is indeed the case: the orientational order parameter S, defined as an average in the nematic phase over the second Legendre polynomial $\mathcal{P}_2(\cos\theta)=(3\cos^2\theta-1)/2$,

$$S=\int dl\, \widetilde{d\theta}\, P^N(l)P^N(\theta|l)\mathcal{P}_2(\cos\theta)$$

is almost indistinguishable from 1 above the discontinuity in the nematic shadow curve, implying that the typical angles θ that the rods make with the nematic axis are very small. This also implies that the rods we consider must be rather thin for Onsager's second virial approximation to be valid: for monodisperse rods [30], the criterion is $D/L \ll \theta$. We return to this point in Sec. IV C.

The results shown above for the finite cutoff regime leave open a number of questions. For example, we observed that both the isotropic cloud and nematic shadow curves move to lower densities as the cutoff increases, but the modest l_m values used are too small to determine whether the curves will converge to a nonzero limit as l_m grows large or instead approach zero. One would also like to ascertain whether the average rod length in the nematic shadow really tends to l_m for large cutoffs, as suggested by Fig. 3, and what happens to the rescaled nematic volume fraction ρ_1^N in this limit (Fig. 2 suggests that it might become large). In the following section, we therefore turn to a theoretical analysis of the limit $l_m\to\infty$, which will clarify all these points.

IV. THEORY FOR FAT-TAILED DISTRIBUTIONS WITH LARGE CUTOFF

Above we saw that, at the onset of isotropic-nematic phase coexistence in systems with log-normal length distri-

butions, the nematic shadow phase appears to be dominated by the longest rods in the distribution, with lengths $l \approx l_m$. In this section, we will construct a self-consistent theory, based on this hypothesis, for the phase behavior in the limit of large cutoffs l_m. From this we will be able to extract the limiting dependence on l_m of the cloud point density ρ, the density ρ^N, and (scaled) volume fraction ρ_1^N of the nematic shadow phase, and the function $g(\theta)$ determining the orientational ordering of the nematic phase. At the end of this section, we will then compare these predictions with numerical results obtained for finite but large cutoff.

A. Dominance of long rods in the nematic phase

Recall that, in principle, we need to solve Eqs. (12) and (13) for $g(\theta)$ and ρ to determine the isotropic cloud point and the properties of the coexisting nematic shadow phase. It will be useful to isolate, in Eq. (12), the contribution $e^{lg(0)}$ that determines the divergence of the nematic density distribution (14). Define the function

$$h(\theta) = l_m[g(0) - g(\theta)] \tag{17}$$

with the sign chosen such that $h(\theta)$ should be non-negative for all θ. Equation (12) evaluated at $\theta = 0$ then gives

$$g(0) = -\rho \int dl\ P^{(0)}(l) e^{lg(0)} l \int \widetilde{d\theta'} e^{-(l/l_m)h(\theta')} K(0,\theta') + c_1\rho, \tag{18}$$

and subtracting from Eq. (12) yields

$$h(\theta) = \rho l_m \int dl\ P^{(0)}(l) e^{lg(0)} l \times \int \widetilde{d\theta'} e^{-(l/l_m)h(\theta')} [K(\theta,\theta') - K(0,\theta')]. \tag{19}$$

Together, Eqs. (18) and (19) for $g(0)$ and $h(\theta)$ are, of course, equivalent to Eq. (12) for $g(\theta)$.

To formalize the assumption that the nematic phase is dominated by the longest rods, consider now the nematic density distribution (14), which in our new notation reads

$$\rho^N(l) = \rho P^{(0)}(l) e^{lg(0)} \int \widetilde{d\theta}\ e^{-(l/l_m)h(\theta)}. \tag{20}$$

If the exponential factor $\exp[lg(0)]$ is large enough for the nematic phase indeed to be dominated by the longest rods, we can replace the weakly varying (at most as a power law in l) angular integral by its value at $l = l_m$, giving for the nematic density $\rho^N = \int dl\ \rho^N(l)$

$$\rho^N = \rho \int dl\ P^{(0)}(l) e^{lg(0)} \int \widetilde{d\theta}\ e^{-h(\theta)}. \tag{21}$$

We can now make the same approximation in Eq. (18): the weakly varying factor in the l integral is l times the angular integral, and replacing this by its value at $l = l_m$ yields

$$g(0) = -\rho l_m \int dl\ P^{(0)}(l) e^{lg(0)} \int \widetilde{d\theta}\ e^{-h(\theta)} K(0,\theta) + c_1\rho. \tag{22}$$

In Eq. (19) for $h(\theta)$, the analogous approximation gives

$$h(\theta) = \rho l_m^2 \int dl\ P^{(0)}(l) e^{lg(0)} \times \int \widetilde{d\theta'} e^{-h(\theta')} [K(\theta,\theta') - K(0,\theta')]. \tag{23}$$

Finally, consider the expression on the right-hand side (rhs) of Eq. (13) for the osmotic pressure Π^N in the nematic. The first term is the ideal contribution, i.e., the nematic density ρ^N, while inserting definition (17) in the second term gives

$$\Pi^N = \rho^N - \frac{\rho}{2} \int dl\ P^{(0)}(l) e^{lg(0)} l \times \int \widetilde{d\theta} e^{-(l/l_m)h(\theta)} \left[-\frac{1}{l_m} h(\theta) + g(0) - c_1\rho \right]. \tag{24}$$

Replacing l by l_m in the weakly varying terms then yields

$$\Pi^N = \rho^N - \frac{\rho}{2} \int dl\ P^{(0)}(l) e^{lg(0)} \times \int \widetilde{d\theta}\ e^{-h(\theta)} \{ -h(\theta) + l_m[g(0) - c_1\rho] \}. \tag{25}$$

We show in Appendix B that *a posteriori* the approximation of dominance of the long rods can be justified in all cases above, with the contributions to the l integrals from rod lengths $l \ll l_m$ becoming negligible for $l_m \to \infty$.

B. The large-cutoff scaling solution

We have now got four equations to be solved for ρ^N, $g(0)$, $h(\theta)$ and ρ, appropriately simplified using the assumption that the nematic phase is dominated by the longest rods in the parent distribution. These are Eqs. (21)–(23) and the pressure equality $\Pi^N = \rho + (c_1/2)\rho^2$, with Π^N from Eq. (25). Using Eq. (21), Eq. (23) can be written as

$$h(\theta) = \rho_{\text{eff}} \frac{\int \widetilde{d\theta'} e^{-h(\theta')} [K(\theta,\theta') - K(0,\theta')]}{\int \widetilde{d\theta'} e^{-h(\theta')}}. \tag{26}$$

Here, we have defined

$$\rho_{\text{eff}} = \rho^N l_m^2 \tag{27}$$

which is just the dimensionless density of the nematic phase, with the factor l_m^2 arising from the fact that, since the nematic is effectively monodisperse with $l = l_m$, one should use $l_m L_0$ rather than L_0 in the definition of the unit volume V_0 [see before Eq. (1)]. In the form above, Eq. (26) is identical to Eq. (A4) in Appendix A for a *monodisperse* system at dimensionless density ρ_{eff}. Anticipating that ρ_{eff} will be large, an as-

sumption to be checked *a posteriori*, we then deduce immediately that $h(\theta)$ will be given by the high-density scaling solution sketched in Appendix A, $h(\theta)=\tilde{h}(t)$, with the scaling variable $t=\rho_{\rm eff}\sin\theta$. The scaling function is determined by Eq. (A8):

$$\tilde{h}(t)=\langle \tilde{K}(t,t')-\tilde{K}(0,t')\rangle_{t'}, \tag{28}$$

where the average over t' is over the normalized distribution

$$\tilde{P}(t)=\frac{1}{\gamma}te^{-\tilde{h}(t)}, \quad \gamma=\int dt\ te^{-\tilde{h}(t)}, \tag{29}$$

and $\tilde{K}(t,t')$ is the small-angle scaling form (A7) of the kernel $K(\theta,\theta')$. The range of all averages and integrals over t and t' can be taken as $0\ldots\infty$ (rather than $0\ldots\rho_{\rm eff}$) for large $\rho_{\rm eff}$, since the large t regime gives only a negligible contribution.

With the form of $h(\theta)$ determined up to the single parameter $\rho_{\rm eff}=\rho^N l_m^2$, just three unknowns ρ, ρ^N, and $g(0)$ now remain to be determined from Eq. (21), Eq. (22), and the osmotic pressure equality. We now simplify these relations further making use of the fact that in all angular integrals involving the factor $\exp[-h(\theta)]=\exp[-\tilde{h}(\rho_{\rm eff}\sin\theta)]$ only small angles $\theta\sim 1/\rho_{\rm eff}$ contribute significantly. Physically, this means that the rods in the nematic shadow phase, which is at high dimensionless density $\rho_{\rm eff}$, have strong orientational order. For such small θ we can set $\sin\theta\approx\theta$ and transform everywhere to the scaling variable $t=\rho_{\rm eff}\sin\theta\approx\rho_{\rm eff}\theta$. Equation (21) then becomes, using definition (29)

$$\rho^N=\rho\int dl\ P^{(0)}(l)e^{lg(0)}\int \frac{dt\,t}{\rho_{\rm eff}^2}e^{-\tilde{h}(t)}$$

$$=\frac{\rho\gamma}{\rho_{\rm eff}^2}\int dl\,P^{(0)}(l)e^{lg(0)}. \tag{30}$$

Equation (22) can be similarly transformed and, using $K(0,\theta)=(8/\pi)\sin\theta=(8/\pi)t/\rho_{\rm eff}$, it reads

$$g(0)=-\rho l_m\int dl\,P^{(0)}(l)e^{lg(0)}\int\frac{dt\,t}{\rho_{\rm eff}^2}e^{-\tilde{h}(t)}\left(\frac{8}{\pi}\frac{t}{\rho_{\rm eff}}\right)+c_1\rho. \tag{31}$$

Comparing with Eq. (30), and using $\rho^N l_m/\rho_{\rm eff}=1/l_m$, this can be written in a simpler form as an average over the distribution (29),

$$g(0)=-\frac{8}{\pi}\frac{\langle t\rangle_t}{l_m}+c_1\rho. \tag{32}$$

Finally, expression (25) for the osmotic pressure in the nematic can also be simplified by using that θ is small and transforming to the scaling variable t. Inserting Eq. (32), one finds

$$\Pi^N=\rho^N+\frac{\rho}{2}\int dl\,P^{(0)}(l)e^{lg(0)}\frac{\gamma}{\rho_{\rm eff}^2}\left[\langle\tilde{h}(t)\rangle_t+\frac{8}{\pi}\langle t\rangle_t\right]. \tag{33}$$

In Appendix A, we show [Eq. (A15)] that the scaling properties of the high-density limit imply that the constant in the square brackets has the value 4; using also Eq. (30) we then get the simple result

$$\Pi^N=3\rho^N. \tag{34}$$

This is identical to Eq. (A12) derived in Appendix A for monodisperse nematics at high (dimensionless) densities, and therefore consistent with our assumption that the nematic shadow phase behaves as an effectively monodisperse system. The isotropic parent phase has pressure $\Pi^I=\rho+(c_1/2)\rho^2$, so that the pressure equality takes the form

$$\rho^N=\frac{1}{3}\left(\rho+\frac{c_1}{2}\rho^2\right). \tag{35}$$

We can now proceed to determine the l_m dependence of ρ, ρ^N, and $g(0)$. Multiplying Eq. (30) by $(\rho^N)^2$ and inserting Eq. (35) gives

$$\frac{\rho^3}{27}\left(1+\frac{c_1}{2}\rho\right)^3=\rho\frac{\gamma}{l_m^4}\int dl\,P^{(0)}(l)e^{lg(0)}.$$

The l integral will again be dominated by the longest rods, so that we can set $P^{(0)}(l)=P^{(0)}(l_m)$ to leading order (see Ref. [26]) to obtain

$$\frac{\rho^2}{27}\left(1+\frac{c_1}{2}\rho\right)^3=\frac{\gamma}{l_m^4}P^{(0)}(l_m)\frac{e^{l_m g(0)}}{g(0)}.$$

Inserting Eq. (32) to eliminate $g(0)$, we finally get a nonlinear equation relating ρ and l_m,

$$e^{l_m c_1\rho}=\frac{\rho^2 l_m^4}{27\gamma}\left(1+\frac{c_1}{2}\rho\right)^3\left(c_1\rho-\frac{8}{\pi}\frac{\langle t\rangle_t}{l_m}\right)\frac{e^{(8/\pi)\langle t\rangle_t}}{P^{(0)}(l_m)}.$$

To obtain the asymptotic solution for large l_m, we anticipate that ρ will vary no stronger than a power law with l_m; for all fat-tailed parent distributions, except those with power-law tails, the dominant l_m dependence on the rhs will then be through the factor $1/P^{(0)}(l_m)$. Taking logarithms we have

$$l_m c_1\rho=-\ln P^{(0)}(l_m)+O(\ln l_m). \tag{36}$$

Specializing to log-normal parent distributions, with $\ln P^{(0)}(l)=-(\ln^2 l)/(2w^2)$ to leading order, we finally get

$$\rho=\frac{\ln^2 l_m}{2c_1 w^2 l_m}+O\left(\frac{\ln l_m}{l_m}\right) \tag{37}$$

showing that ρ indeed varies with l_m as a power law (with logarithmic corrections). Our theory thus predicts that the isotropic cloud point density converges to zero for large cutoffs; in the extreme limit of a log-normal parent distribution

with an infinite cutoff, phase separation would occur at any nonzero density. From Eq. (35), the density of the nematic shadow phase likewise vanishes for large cutoff, with $\rho^N = \rho/3$ to leading order. For $g(0)$, we have from Eq. (32),

$$g(0) = \frac{\ln^2 l_m}{2w^2 l_m} + O\left(\frac{\ln l_m}{l_m}\right) - \frac{8}{\pi}\frac{\langle t\rangle_t}{l_m}, \tag{38}$$

and the last term of $O(1/l_m)$ is subdominant compared to both the first term and the first-order correction $O((\ln l_m)/l_m)$. We can also now write down the whole function $g(\theta)$, using $g(\theta) = g(0) - h(\theta)/l_m = g(0) - \tilde{h}(\rho^N l_m^2 \sin\theta)/l_m$. From Appendix A we know that the scaling function $\tilde{h}$ is given by $\tilde{h}(t) = (8/\pi)t$ for large t, up to correction terms of $O(1)$; once multiplied by $1/l_m$, these give only subleading corrections to $g(\theta)$. We thus find to leading order

$$g(\theta) = g(0) - \frac{1}{l_m}\tilde{h}(\rho^N l_m^2 \sin\theta) \simeq a - b\sin\theta, \tag{39}$$

where, using Eq. (37) and the leading-order relation $\rho^N = \rho/3$,

$$a \equiv g(0) = \frac{\ln^2 l_m}{2w^2 l_m} + O\left(\frac{\ln l_m}{l_m}\right) \tag{40}$$

$$b = \frac{8}{\pi} l_m \rho^N = \frac{8}{3\pi}\frac{\ln^2 l_m}{2c_1 w^2} + O(\ln l_m). \tag{41}$$

The dominance of the long rods in the nematic phase thus results in a very simple form for $g(\theta)$, with a vanishing and b slowly diverging in the limit $l_m \to \infty$.

Having obtained the desired predictions from our theory, we can now also verify that the assumption of a large dimensionless density ρ_{eff} for the nematic phase is self-consistent. From Eq. (37) and the fact that to leading order $\rho^N = \rho/3$, one has $\rho_{\text{eff}} = \rho^N l_m^2 \sim l_m \ln^2 l_m$ for a log-normal parent distribution, and this indeed becomes arbitrarily large as the cutoff l_m increases.

C. Validity of Onsager theory

Before comparing our theoretical predictions with numerical results at finite cutoff, we briefly assess the limit of validity of Onsager's second virial approximation. For a monodisperse system, an analysis of the scaling of the second and third virial coefficients [30] shows that in the nematic phase, typical rod angles θ with the nematic axis have to be $\gg D/L$, with D and L the diameter and length of the rods, for the truncation after the second virial contribution to be justified. In our situation, the nematic phase is effectively monodisperse with (unnormalized) rod length $L_0 l_m$, so the condition becomes $\theta \gg D/(L_0 l_m)$. We showed above that the typical angles scale, for large cutoff l_m, as $\theta \sim 1/\rho_{\text{eff}} = 1/(\rho^N l_m^2)$, so that the second virial approximation breaks down when

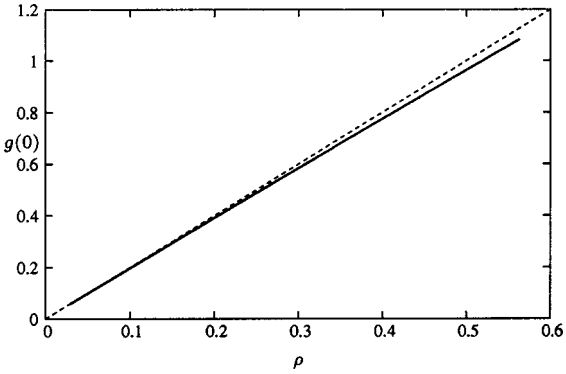

FIG. 4. Parametric plot of $g(0)$ against ρ, for a log-normal distribution with $\sigma = 0.5$ and a range of cutoffs between 50 and 3000. At small ρ (large l_m), the numerical results (solid) are in very good agreement with the theoretically predicted asymptotic relation $g(0) = c_1\rho$ (dashed).

$$\frac{D}{L_0 l_m} \sim \frac{1}{\rho^N l_m^2}. \tag{42}$$

Now ρ^N scales as $(\ln^2 l_m)/l_m$, so this becomes $\ln^2 l_m \sim L_0/D$. This shows that fairly large values of the aspect ratio L_0/D of the "reference rods" are necessary in order for the theory to be valid for large cutoffs. For instance, one would need $L_0/D \simeq 50$ for a cutoff $l_m = 1000$. The longest rods are then very thin indeed, with $L_0 l_m/D \simeq 50\,000$.

A more physically intuitive interpretation of the above condition is that it corresponds to the requirement of having a rod volume fraction $\phi \ll 1$. For monodisperse rods, we have (see Appendix A) that at large dimensionless density ρ, $\theta \sim \rho^{-1} \sim (L^2 DN/V)^{-1}$. The limit of validity of the Onsager theory is therefore given by $D/L \sim \theta \sim V/(L^2 DN)$ or $1 \sim (LD^2 N)/V \sim \phi$. The same is true for our calculation above: the volume fraction of the nematic phase is $\phi^N = (D/L_0)\rho_1^N \simeq (D/L_0) l_m \rho^N$. Condition (42) thus again becomes $\phi^N \sim 1$, and we need $\phi^N \ll 1$ for the second virial theory to be valid.

D. Comparison with numerical results

We now compare the theoretical predictions obtained above for the limit $l_m \to \infty$ with numerical calculations for finite but large cutoff. Our numerical results will be able to confirm only the leading terms of the scaling solution, since subleading corrections [e.g., to result (39) for $g(\theta)$] can arise from the regime of very small angles $\theta \sim 1/\rho_{\text{eff}} = 1/(\rho^N l_m^2)$, which we cannot resolve numerically.

We begin by checking the predicted relations between the cloud point density ρ and the other quantities we have analyzed theoretically, namely, the parameters a and b specifying the leading behavior (39) of $g(\theta)$, and the nematic shadow density ρ^N. In Fig. 4, we plot $g(0) \equiv a$ against ρ for a range of cutoffs l_m between 50 and 3000. At large cutoff, i.e., at small ρ, the numerical results are clearly seen to approach the theoretical prediction $g(0) = c_1\rho$, while for smaller cutoffs deviations from the asymptotic theory appear as expected.

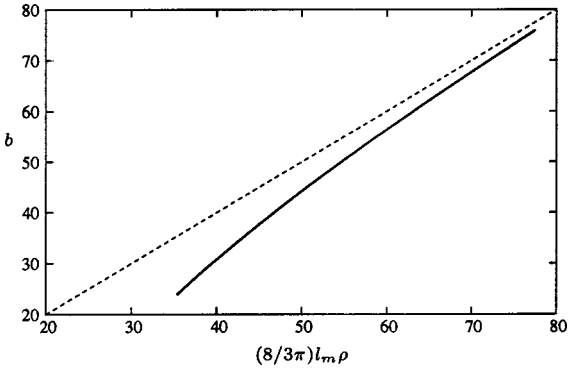

FIG. 5. Parametric plot of b against the theoretically predicted value $(8/3\pi)l_m\rho$ for a log-normal distribution with $\sigma=0.5$ and cutoff between 50 and 3000. The convergence of the numerical results (solid) to the theoretical prediction (dashed) for large cutoff, i.e., large $l_m\rho$, is clear.

For the parameter b, our theory predicted $b=(8/3\pi)l_m\rho$ in the limit of large l_m. In Fig. 5, we plot the numerically obtained b against this theoretical prediction, for a range of cutoffs between 50 and 3000. At large $l_m\rho$ the convergence to the theoretical solution is clear, while at finite cutoff (small $l_m\rho$) the value of b lies rather below the theoretical expectation. This is not surprising, since b is expected to diverge with l_m like $\ln^2 l_m$ and therefore rather slowly; at finite cutoff, then, the correction terms will be rather important.

Based on the fact that the nematic pressure obeys the simple relation $\Pi^N=3\rho^N$ in the large-cutoff limit, our theory also predicts that ρ^N should be related to ρ by $\rho^N=[\rho+(c_1/2)\rho^2]/3=(\rho+\rho^2)/3$. A plot of ρ^N against ρ for the same range of cutoffs as above (Fig. 6) clearly shows that this relation is satisfied in the limit of large l_m, i.e., small ρ. In fact, deviations from the predicted scaling are rather small, already at modest l_m (here, in the range $50\leqslant l_m\leqslant 3000$). This shows that the dominance of the long rods, demonstrated also by the fact that the average length of the nematic phase is very close to l_m (Fig. 3), appears quite early on. Even at $l_m=50$, not only is the nematic phase composed

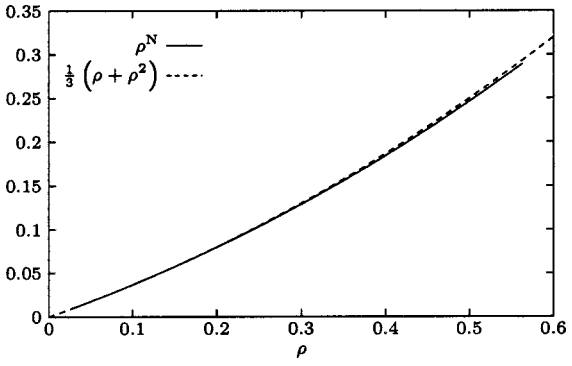

FIG. 6. Parametric plot of the nematic shadow density ρ^N against ρ for the same parent distribution and cutoff range as in Figs. 4 and 5. A very good agreement is observed between the numerical results (solid) and the theoretically predicted relation (dashed).

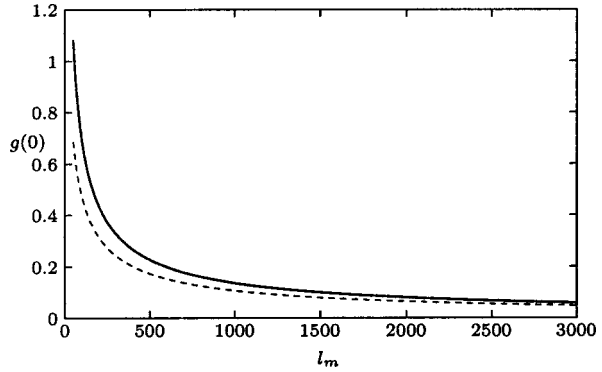

FIG. 7. Plot of numerically calculated values of $g(0)$ against l_m (solid) together with the leading asymptotic behavior $g(0)=(\ln^2 l_m)/(2w^2 l_m)$ predicted theoretically (dashed) for a log-normal distribution with $\sigma=0.5$. The agreement is satisfactory, though corrections to the asymptotic theory are clearly still important in the range of l_m shown.

almost entirely of rods of the order of l_m, but the rods are also sufficiently strongly ordered to make our scaling solution a good approximation.

Having confirmed the relations between a, b, ρ, and ρ^N, the last prediction to verify is the variation of one of these quantities with l_m. We choose $a\equiv g(0)$, for which our theory predicts the leading asymptotic behavior $g(0)=(\ln^2 l_m)/(2w^2 l_m)$. In Fig. 7, we plot the numerically calculated values of $g(0)$ versus l_m and compare with the theoretical prediction. The overall shape of the l_m dependence is well captured by the theory, although subleading corrections, which from Eq. (38) are of relative order $O(1/\ln l_m)$, are clearly not yet negligible in the range of l_m considered. In summary, then, all numerical results are consistent with the theoretical predictions derived above.

V. THE SCHULZ DISTRIBUTION

Having observed the rather surprising effects caused by the long rods at the onset of isotropic-nematic coexistence in systems with fat-tailed length distributions, an obvious question is whether similar phenomena are possible even for more strongly decaying length distributions. We therefore now analyze, using the same numerical and theoretical methods as above, the case of a Schulz distribution of lengths. For this distribution, our previous studies of the Zwanzig [18] and $\mathcal{P}_2$ Onsager models [27] did not show any signs of the phase behavior being driven by the long rods. However, comparing our above results for the log-normal case with those obtained for the $\mathcal{P}_2$ Onsager model [26], it is clear that in the full Onsager theory the effect of the long rods is much more pronounced than in the approximate models. Long-rod effects might therefore also appear, in the full Onsager theory, for the more strongly decaying Schulz distribution, but would then be expected to be weaker than for the log-normal case.

The Schulz length distribution can be written as

$$P^{(0)}(l)=\frac{(z+1)^{z+1}}{\Gamma(z+1)}l^z\exp[-(z+1)l], \qquad (43)$$

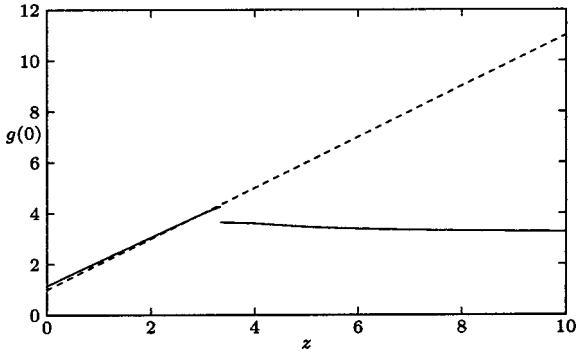

FIG. 8. The parameter $g(0)$ of the nematic shadow phase plotted against z for a Schulz distribution with cutoff $l_m=100$. See text for discussion.

where we have again imposed an average length of 1 (for infinite cutoff l_m). The polydispersity σ, defined as before as the relative standard deviation of the distribution, is related to z by

$$\sigma^2=\frac{\langle l^2\rangle-\langle l\rangle^2}{\langle l\rangle^2}=\frac{1}{z+1}. \tag{44}$$

From Eqs. (14) and (43) it is clear that if $g(0)\geqslant z+1$ the nematic density distribution is again exponentially diverging for large l. Assuming initially that this is not the case, however, one can solve numerically Eqs. (12) and (13) for the onset of isotropic-nematic phase coexistence. The results for $g(0)$ are shown in Fig. 8. For large z, i.e., small polydispersity $\sigma=(1+z)^{-1/2}$, one has $g(0)<z+1$ (dashed line). In this regime, the nematic density distribution decays exponentially for large l, and the results are essentially independent of the cutoff l_m, which could in fact be taken to infinity. For smaller z, on the other hand, $g(0)>z+1$, implying that the nematic density distribution is exponentially increasing and a finite cutoff l_m is necessary. In this regime, the situation resembles the case of the fat-tailed length distributions discussed earlier, where for a large enough cutoff and polydispersity, the less than exponentially decaying length distribution was not able to balance the divergence of the factor $\exp[lg(0)]$ in Eq. (14). With a Schulz distribution, the only difference is that now the comparison is between two exponential terms $\exp[-(z+1)l]$ and $\exp[lg(0)]$. Given this analogy, it is not surprising that the cloud and shadow curves (Fig. 9) show a behavior qualitatively similar to that found for the log-normal distribution: a kink in the cloud curve and a discontinuity in the shadow curve again indicate the presence of a three-phase I-N-N coexistence region in the phase diagram. Quantitatively, however, the kink in the cloud curve [Fig. 9(a)] is now much less pronounced, and the cutoff-dependence of the cloud curve above the kink is also rather weaker. Similar comments apply to the shadow curve [Fig. 9(b)]: the discontinuity is still present but very small, with the nematic phases on the two different branches having very similar densities [Fig. 9(b), inset]. As for the log-normal distribution, for small polydispersities (i.e., below the kink or discontinuity, respectively) the cloud and shadow curves are

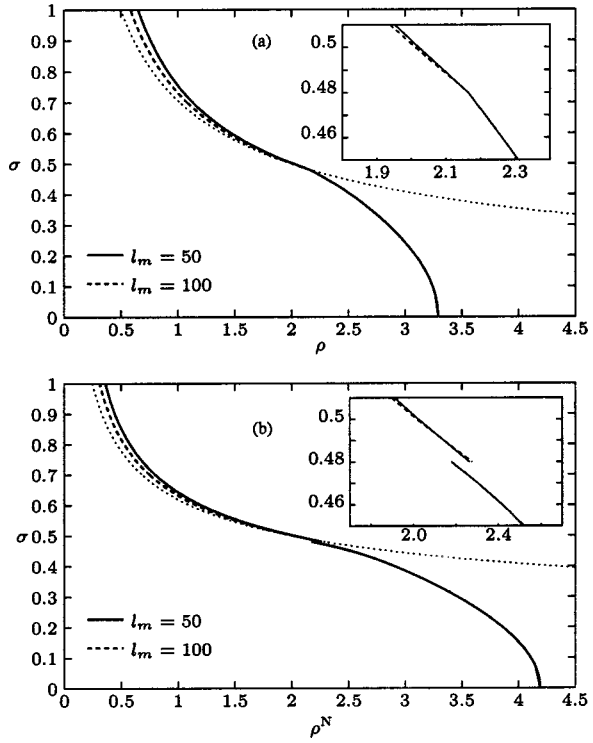

FIG. 9. (a) Cloud curves for Schulz distributions with cutoff $l_m=50$ (solid) and $l_m=100$ (dashed) plotted as cloud point density ρ versus polydispersity σ on the y axis. The system is again dominated by the long rods for large σ, but now the dependence on the cutoff is much less pronounced than for a log-normal length distribution (Fig. 1). The cloud curves also exhibit a kink, more clearly visible only on a magnified scale (inset). The dotted line shows the theoretically predicted limiting form $\rho=1/(c_1\sigma^2)$ of the cloud point curve above the kink (see text) in the limit $l_m\to\infty$. (b) Corresponding shadow curves. The discontinuity corresponding to the kink in the cloud curves is much narrower than in the log-normal case (Fig. 1), and is visible clearly only in the inset. The dotted line again gives the theoretical prediction for the shadow curve above the discontinuity in the limit $l_m\to\infty$, $\rho^N=(1/\sigma^2+1/2\sigma^4)/(3c_1)$.

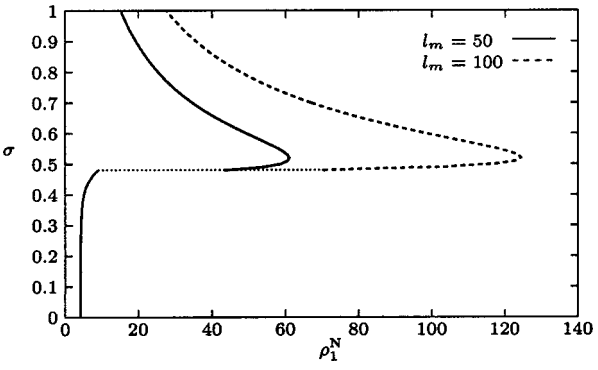

FIG. 10. Scaled volume fraction representation of the shadow curve for Schulz distributions with cutoff $l_m=50$ (solid) and $l_m=100$ (dashed). Notice that, although the discontinuity is much more visible here than in the density representation [Fig. 9(b)], the maximum value of ρ_1^N is not reached at the discontinuity.

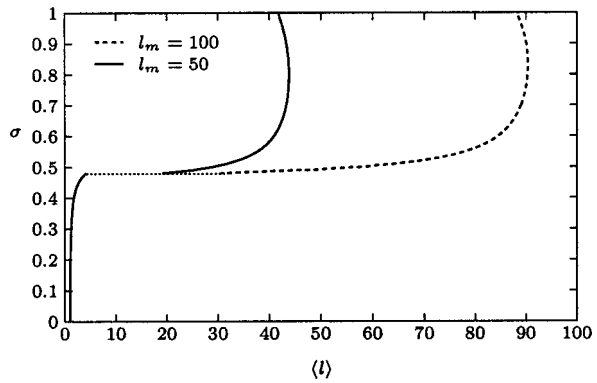

FIG. 11. Average rod length in the nematic shadow phase for Schulz distributions with cutoff $l_m=50$ (solid) and $l_m=100$ (dashed), plotted against polydispersity σ on the y axis. Above the discontinuity, the average length jumps to a large value but remains below l_m, implying that the nematic phase is not yet entirely dominated by the longest rods.

essentially independent of the cutoff and connect smoothly with the monodisperse limit at $\sigma=0$.

The discontinuity in the shadow curves is much more apparent in the scaled volume fraction representation (Fig. 10). Notice that now the discontinuity does not coincide with the point where ρ_1^N reaches its maximum value, as was the case for the log-normal distribution (Fig. 2). This is also reflected in a plot of the average rod length in the nematic shadow against polydispersity (Fig. 11), which at the discontinuity in the shadow curve jumps to a large value, but one that is still some way below l_m. In this region, the nematic phase thus contains many long rods, but is not yet entirely dominated by only the longest rods. This can also be understood by looking back at Fig. 8: for values of z just below the discontinuity (corresponding to the values of σ just *above* the discontinuity in Figs. 10 and 11), $g(0)$ is very close to $z+1$ and so the overall exponential factor $\exp\{[g(0)-(z+1)]l\}$ is almost constant over the range $l=0 \ldots l_m$, giving a broad nematic length distribution (14) dominated by the nonexponential factors $l^z \int \widetilde{d\theta}\, e^{l[g(\theta)-g(0)]}$.

Theory for Schulz distributions with large cutoff

From the numerical results obtained above, it appears that the case of the Schulz distribution is actually rather similar to the log-normal case. In both cases, the presence of the long rods strongly affects the phase behavior above a certain value of polydispersity σ; the threshold value of σ tends to zero as l_m increases for the log-normal case, but appears essentially independent of l_m for the Schulz distribution. Above the threshold, the nematic phase is dominated by the long rods present in the system, although for the Schulz distribution the average length seems to remain rather below l_m. Given these similarities, we now investigate whether the theory that we developed for the log-normal case can be extended to the case of the Schulz distribution. As we will see, the central assumption of dominance of the long rods in the nematic phase can still be made self-consistent.

If the long rods again dominate the density distribution in the nematic phase, we can repeat all the steps up to Eq. (25) in Sec. IV. The same equation for $h(\theta)$ follows, and if we assume that $\rho_{\mathrm{eff}}=\rho^N l_m^2$ is large we get back the scaling solution $h(\theta)=\tilde{h}(\rho_{\mathrm{eff}}\sin\theta)$. Angular integrals can then again be simplified because only small values of $\theta \sim 1/\rho_{\mathrm{eff}}$ are relevant, leading to Eq. (30), to the simple result $\Pi^N=3\rho^N$ for the osmotic pressure in the nematic phase, and to expression (32) for $g(0)=c_1\rho-(8/\pi)\langle t\rangle_t/l_m$. At this point the different shape of the Schulz distribution enters: for large l_m we now expect that $g(0)\to z+1$, rather than $g(0)\to 0$. This then implies that the cloud point density ρ has a *finite* limit for large cutoff, given by

$$\rho=\frac{z+1}{c_1}=\frac{1}{c_1\sigma^2} \tag{45}$$

from Eq. (44). From the osmotic pressure equality $3\rho^N=\rho+(c_1/2)\rho^2$, the nematic shadow density then also has a finite limit,

$$\rho^N=\frac{1}{3c_1}\left(\frac{1}{\sigma^2}+\frac{1}{2\sigma^4}\right). \tag{46}$$

These theoretical predictions for the limiting form of the cloud and shadow curves in the cutoff-dominated regime are shown by the dotted lines in Fig. 9, and are certainly plausible, given the numerical results for finite cutoffs.

To obtain the leading terms in the approach of ρ and ρ^N to their limiting values, and to establish the threshold value of polydispersity σ above which the onset of I-N coexistence is affected by the presence of the long rods, let us define $\delta=g(0)-(z+1)$. As pointed out above, Eq. (30) still holds for the Schulz distribution case, but now yields to leading order

$$\rho^N=\frac{c}{l_m^4}\int dl\, l^z e^{\delta l}, \tag{47}$$

where we have used $P^{(0)}(l)\propto l^z e^{-(z+1)l}$ and c collects all numerical constants as well as the factor $\rho/(\rho^N)^2$ that approaches a constant for $l_m\to\infty$ from Eqs. (45) and (46). If δ converges to zero slowly enough with $l_m\to\infty$ for the product δl_m to diverge, then the exponential factor is dominant in the integral in Eq. (47) and we can replace l^z by l_m^z (see Appendix C) to get

$$\rho^N=c\, l_m^{z-4}\frac{e^{\delta l_m}}{\delta}.$$

Rearranging gives, with a new constant c' that contains the finite limit value of ρ^N,

$$\frac{e^{\delta l_m}}{\delta l_m}=c'\, l_m^{3-z}.$$

The inverse of the function of δl_m on the left-hand side is asymptotically just a logarithm, yielding

$$\delta \sim (3-z)\frac{\ln l_m}{l_m}. \tag{48}$$

For $z<3$, corresponding to $\sigma>1/2$, this result is consistent with our assumptions: we have $\delta \to 0$ and thus $g(0) \to z+1$ as expected, and also $\delta l_m \to \infty$ as assumed above. From the convergence of δ to zero one can then also obtain the approach of ρ and ρ^N to their limit values: e.g., $c_1\rho = g(0) + (8/\pi)\langle t\rangle_t / l_m = z+1+\delta+O(1/l_m)$, giving $\rho-(z+1)/c_1 \sim \delta$ to leading order.

From the above results, we can furthermore estimate the average rod length in the nematic shadow phase for $z<3$ and finite l_m. The exponential factor $\exp(\delta l)$ dominates the nematic density distribution and so rods in a range of $O(1/\delta)$ below l_m should contribute to the average length, giving the estimate

$$\langle l\rangle^N = l_m\left[1-O\left(\frac{1}{\delta l_m}\right)\right] = l_m\left[1-O\left(\frac{1}{\ln l_m}\right)\right].$$

This shows that there are strong logarithmic corrections, consistent with the fact that in Fig. 11 the average nematic rod lengths $\langle l\rangle^N$ are still significantly below l_m. By contrast, in the log-normal case, where the role of δ is played by $g(0)$, the relative corrections to $\langle l\rangle^N$ are $\sim 1/(g(0)l_m) \sim 1/\ln^2 l_m$; even though still logarithmic, these correction terms are significantly smaller.

Overall, the behavior of ''wide'' Schulz distributions with $\sigma>1/2$, i.e., $z<3$, is therefore rather similar to that of log-normal distributions. We again have $\langle l\rangle^N \to l_m$ for large l_m, although now the corrections are rather more important than in the previous case, and the rods in the nematic phase are strongly ordered (since $\rho_{\rm eff}=\rho^N l_m^2 \sim l_m^2$ diverges for $l_m \to \infty$). The main difference is the fact that the cloud and shadow densities, ρ and ρ^N, now tend to distinct nonzero limits for $l_m \to \infty$ rather than to zero: the smaller number of long rods in the Schulz distribution is not sufficient to induce phase separation at arbitrarily small densities.

So far, we have only covered the regime $z<3$. The case $z=3$ requires a more careful treatment; here the leading contribution to δ calculated in Eq. (48) vanishes, and it turns out that δ scales as $1/l_m$, with δl_m approaching a finite limit rather than diverging. Rods in the range $\sim 1/\delta \sim l_m$ now contribute to the nematic density distribution, which therefore is no longer dominated by the longest rods alone even for $l_m \to \infty$; instead, one finds that the distribution approaches a scaling function of l/l_m, with the ratio $\langle l\rangle^N/l_m$ tending to a nontrivial limit value <1.

In the case $z>3$, finally, we cannot construct a self-consistent theory based on the assumption that the nematic phase is dominated by long rods. Looking at Eq. (47), one sees that for $z>3$ *negative* values of δ would be required to make the rhs of the equation (and thus ρ^N) finite for $l_m \to \infty$; with such negative values of δ, the assumption of dominance of the long rods in the nematic phase is no longer self-consistent. One might try the milder assumption that the nematic is dominated by rods that are long but still short compared to l_m, assuming, e.g., $\langle l\rangle^N \sim l_m^\alpha$, with $\alpha<1$. We found, however, that this always leads to contradictions. Our conclusion is therefore that for $z>3$, i.e., $\sigma<1/2$, the nematic phase is dominated by ''short'' rods with lengths not increasing with l_m. The theoretically predicted threshold value of σ below which the cutoff l_m is irrelevant and the presence of long rods in the system does not significantly affect the phase behavior is therefore $\sigma=1/2$.

Our numerical results (Fig. 9) show the kink in the cloud curve, and the corresponding discontinuity in the shadow curve at $\sigma \approx 0.48$, i.e., close to but slightly below the theoretically predicted threshold value. Comparing with Fig. 8, this corresponds to the fact that, coming from large z, the discontinuous jump in $g(0)$ occurs before the extrapolation of the solution in the large-z regime intersects the critical line $g(0)=z+1$; consistent with our theory, and extrapolating by eye, this intersection occurs close to $z=3$. It therefore appears that for finite l_m the shadow curve jumps to a cutoff-dependent branch, i.e., a nematic containing many long rods, already slightly below the asymptotic threshold value $\sigma=1/2$. The value of σ where this jump occurs should then increase towards 1/2 as l_m increases.

VI. CONCLUSION

We have studied the effect of length polydispersity on the onset of *I-N* phase coexistence in the Onsager theory of hard rods. To assess the possible effects of long rods, two different length distributions were considered, one with a slowly decaying, fat tail (log-normal) and another with an exponentially decaying tail (Schulz).

We showed that a length cutoff l_m needs to be introduced for fat-tailed distributions such as the log-normal to avoid divergences in the equations for the onset of phase separation; the presence of such a cutoff is, of course, also physically reasonable. The most striking result from our numerical solution for the properties of the isotropic cloud and nematic shadow phases is that the cloud curves show a kink and the shadow curves corresponding discontinuities: this establishes that for fat-tailed *unimodal* length distributions, three-phase *I-N-N* coexistence occurs. The cloud and shadow curves show a strong dependence on the cutoff length, with both moving rapidly to lower densities as the cutoff increases. A plot of the average rod length suggested that the nematic shadow phase consists almost entirely of the longest rods in the system, i.e., those of length l_m; as a result, it also exhibits very strong orientational ordering.

A theoretical analysis of the limiting behavior for $l_m \to \infty$ confirmed and extended these numerical results. For large cutoffs, the nematic indeed comprises only the longest rods in the parent length distribution, and is very strongly ordered. Beyond this, the theory also predicts that the densities of the isotropic cloud and nematic shadow phases in fact *vanish* (with constant ratio $\rho/\rho^N=3$) in the limit of infinite cutoff. This rather surprising result means that even though the *average* rod length in the parent distribution is finite, the fat tail of the distribution ensures that enough arbitrarily long rods are present to induce phase separation at any nonzero density. Even though the nematic shadow density converges to zero for increasing l_m, it does so slowly enough [ρ^N

$\sim(\ln^2 l_m)/l_m]$ for the rescaled rod *volume fraction* of the nematic to *diverge* logarithmically with l_m ($\rho_1^N \sim \ln^2 l_m$). For any given aspect ratio of rods, the Onsager second virial approximation thus eventually breaks down as l_m increases, at the point where the true volume fraction $(D/L_0)\rho_1^N$ of the nematic shadow becomes non-negligible compared to unity.

We then studied numerically the case of a Schulz distribution of rod lengths, for which our previous studies of the simplified Zwanzig [18] and $\mathcal{P}_2$ Onsager models [27] showed no *I-N-N* coexistence and no unusual behavior in the limit of infinite rod length cutoff. The full Onsager theory studied here revealed, however, that such effects do indeed occur: above a threshold value of the polydispersity σ, the numerical results show that the nematic density distribution becomes exponentially divergent for large rod lengths; a finite cutoff l_m again needs to be imposed to get meaningful results. Above the threshold, the cloud and shadow curves then depend on l_m, although much more weakly than in the log-normal case. The dominance of the long rods in the nematic shadow phase above the threshold is also weaker than for the log-normal, with average rod lengths that are large but significantly below l_m. At the threshold itself, a kink in the cloud curve and a discontinuity in the shadow curve occur, indicating that even for the ''well-behaved'' Schulz distribution the Onsager theory predicts a three-phase *I-N-N* phase coexistence region in the phase diagram.

We were again able to clarify these results by theoretical analysis of the limit $l_m \to \infty$. We found that the limiting threshold value of the polydispersity is $\sigma = 1/2$, corresponding to an exponent $z = 3$ in the Schulz distribution, in good agreement with the numerically calculated thresholds at small cutoffs. Above the threshold value, the theory predicts that the average nematic rod length approaches l_m as in the log-normal case, but now with larger logarithmic corrections that explain the smaller average lengths observed numerically. In contrast to the log-normal distribution, the cloud and shadow curves above the threshold approach *finite* limiting values for $l_m \to \infty$. The physical interpretation is that the smaller number of long rods in the Schulz distribution is not sufficient to induce a phase separation at arbitrarily small densities.

It is appropriate at this stage to compare the above results with our earlier analysis of the $\mathcal{P}_2$ Onsager model [26]. For the Schulz distribution we have mentioned already that the $\mathcal{P}_2$ Onsager model, in contrast to the full Onsager theory, predicts no unusual effects (*I-N-N* coexistence and cutoff dependences) due to the presence of long rods. For the log-normal distribution, the $\mathcal{P}_2$ Onsager model does exhibit a three-phase *I-N-N* coexistence, with cloud curves showing a kink and shadow curves showing a corresponding discontinuity. As in the full Onsager theory, above the kink the cloud curves are also strongly dependent on the cutoff value. However, the limiting behavior of cloud and shadow curves is rather different: both the densities and the rescaled rod volume fractions of the isotropic cloud and nematic shadow phases converge to finite, and in fact identical, limiting values for a large cutoff. The nematic was also not dominated by the longest rods. In fact, the isotropic and nematic phases differed only through a larger fraction of long rods contained in the nematic, and the shorter rods show only a negligible order in the nematic, with the overall orientational order parameter vanishing in the limit.

The above differences between the predictions of the $\mathcal{P}_2$ Onsager model and the full Onsager theory can be understood as follows. In the Onsager theory, the excluded volume of two rods vanishes as the angle between the rods decreases to zero; this favors strongly ordered nematics such as the nematic shadow phase dominated by long rods that we found at the onset of phase coexistence. In the $\mathcal{P}_2$ Onsager model, on the other hand, and indeed in any similar truncation of the expansion of the kernel $K(\theta, \theta')$ in Legendre polynomials [27], the excluded volume remains nonzero even for two rods fully aligned with the nematic axis. This disfavors nematic phases containing a substantial number of long and strongly ordered rods. It thus makes sense that the nematic shadow phase even for the fat log-normal distribution is predicted to contain only a small (though enhanced as compared to the isotropic phase) fraction of long rods.

Looking back over our results for the effects of length polydispersity in the full Onsager theory, it is clear that all the effects of long rods that we observe arise from the exponential factor $\exp[lg(0)]$ [(see Eq. (14)] which dominates the enhancement of the nematic shadow phase density distribution over that of the isotropic parent phase. Any parent length distribution with a less than exponentially decaying fat tail will therefore exhibit divergences in the nematic distribution, leading to a phase behavior similar to that for the log-normal case. In fact, our theory in Sec. IV applies to all such fat-tailed distributions. The Schulz distribution with its exponential tail is the borderline case, where one cannot predict *a priori* whether the presence of long rods will have significant effects. We found that it does, above a threshold value of the polydispersity. To our knowledge, this is the first time that such a threshold effect has been observed in polydisperse phase equilibria. (In the Flory-Huggins theory for homopolymers with chain length polydispersity, for example, where the enhancement factor is also a linear exponential—in chain length—no long-rod effects are found for Schulz distributions [24,25].) Finally, for parent rod length distributions decaying more than exponentially, e.g., as $\sim\exp(-l^\alpha)$ with $\alpha > 1$, no cutoff dependences are expected since the nematic density distribution will always be well behaved for large lengths. Of course, this does not mean that the *I-N-N* phase coexistence is excluded for such distributions. Consider, for example, a log-normal length distribution modulated by a Gaussian factor $\exp[-l^2/(2l_m^2)]$ with large l_m. As we just saw, there is then no need for an explicit cutoff. On the other hand, the Gaussian factor will act as an effective ''soft'' cutoff (hence the notation l_m). For large enough l_m, one thus expects a phase behavior qualitatively similar to that discussed above for a ''hard'' cutoff, including the *I-N-N* phase coexistence signaled by a kink in the cloud curve.

Above, we have focused exclusively on the onset of the phase coexistence; both numerically and theoretically the analysis of the phase behavior inside the coexistence region would be far more challenging. One question one would like to answer concerns the overall phase diagram topology. On

the one hand, the three-phase *I-N-N* region could be confined to a narrow density range inside the *I-N* coexistence region, as is the case for the $\mathcal{P}_2$ Onsager model with a log-normal length distribution [26]. The alternative would be for the *I-N-N* region to extend all the way across the *I-N* coexistence region, connecting to the nematic cloud curve and being bordered by a region of *N-N* coexistence; this is predicted by the Onsager theory for bidisperse systems [20,23]. Apart from a direct numerical attack on the phase coexistence region, which for now seems out of reach, clues to an answer could be provided by an approach based on the Flory lattice model of hard rods [31]. For the scenarios studied in the past this has yielded results qualitatively similar to the Onsager theory [19,32,33], in spite of the rather crude treatment of the orientational entropy. Preliminary work shows that, in the limit of thin rods, Flory's excess free energy corresponds to an excluded volume term that correctly tends to zero for small rod angles. Together with the full expression for the ideal part of the free energy, this can be shown to give a scaling behavior in the limit of strong ordering (i.e., high density) very similar to that of the full Onsager theory. This version of the Flory lattice model may therefore produce predictions that are more in qualitative accord with the Onsager theory than, e.g., the $\mathcal{P}_2$ Onsager model. It shares with the latter the desirable feature of being ''truncatable,'' having an excess free energy that depends only on two moments of the density distribution. This will allow the efficient calculation of phase equilibria using the moment free-energy method [18,27,34–37]; work in this direction is in progress.

APPENDIX A: HIGH-DENSITY SCALING FOR THE MONODISPERSE ONSAGER THEORY

We summarize here the arguments leading to the scaling solution for the angular distribution in nematic phases at high density for the case of monodisperse rods [38]. The relevant free energy is obtained from the polydisperse version (1) by dropping all l integrations and setting $l=1$, giving

$$f=\rho(\ln\rho-1)+\rho\int \widetilde{d\theta}\; P(\theta)\ln P(\theta) + \frac{1}{2}\rho^2\int \widetilde{d\theta}\;\widetilde{d\theta'}P(\theta)P(\theta')K(\theta,\theta'). \tag{A1}$$

This expression needs to be minimized with respect to $P(\theta)$, subject to the normalization condition $\int \widetilde{d\theta}\; P(\theta)=1$ in our usual notation. One obtains

$$P(\theta)=\frac{e^{\psi(\theta)}}{\int \widetilde{d\theta'}e^{\psi(\theta')}} \quad \psi(\theta)=-\rho\int \widetilde{d\theta'}P(\theta')K(\theta,\theta'), \tag{A2}$$

which is the obvious monodisperse version of Eq. (2). Defining the function $h(\theta)=\psi(0)-\psi(\theta)$, which obeys $h(0)=0$, this can be written as

$$P(\theta)=\frac{e^{-h(\theta)}}{\int \widetilde{d\theta'}e^{-h(\theta')}}, \tag{A3}$$

$$h(\theta)=\rho\int \widetilde{d\theta'}P(\theta')[K(\theta,\theta')-K(0,\theta')]. \tag{A4}$$

Now consider the regime of high densities, $\rho\gg 1$. From Eq. (A4), it is clear that for large density, $h(\theta)$ becomes large. $P(\theta)$ then becomes strongly peaked around $\theta=0$ so that the only nonvanishing contribution to the angular integral in Eq. (A4) comes from the range $\theta'\ll 1$. [Here and in the following we use the symmetry of $P(\theta)$ and $h(\theta)$ under $\theta\to\pi-\theta$ to restrict all integrations to the range $\theta=0\ldots\pi/2$.] For $\theta\sim O(1)\gg\theta'$, we can then approximate $K(\theta,\theta')\simeq K(\theta,0)=(8/\pi)\sin\theta$, so that

$$h(\theta)\simeq\frac{8}{\pi}\rho\sin\theta \tag{A5}$$

to the leading order in ρ. This expression will not be valid for small θ, but suggests that in this regime a scaling solution in terms of the scaling variable $t=\rho\sin\theta$ could exist, i.e., $h(\theta)=\tilde{h}(t)$. For consistency with Eq. (A5) for $\theta\sim O(1)$ (and large ρ), the scaling function should then have the leading asymptotic behavior $\tilde{h}(t)=(8/\pi)t$ for large t. Now, written in terms of $\tilde{h}(t)$, Eq. (A4) reads

$$\tilde{h}(t)=\frac{\int \frac{dt'\,t'}{\sqrt{1-(t'/\rho)^2}}e^{-\tilde{h}(t')}\rho[K(\theta,\theta')-K(0,\theta')]}{\int \frac{dt'\,t'}{\sqrt{1-(t'/\rho)^2}}e^{-\tilde{h}(t')}}, \tag{A6}$$

where the integrals are over the range $0\ldots\rho$ and $\theta=\arcsin(t/\rho)$, $\theta'=\arcsin(t'/\rho)$. The key property that allows one to get a density-independent equation for $\tilde{h}(t)$ is the scaling behavior of the kernel. For finite t and t' and large ρ, one has $\theta\approx t/\rho$, $\theta'\approx t'/\rho$, and for such small (and comparable) angles the kernel scales *linearly* with the angles. The product $\rho K(\theta,\theta')=\rho K(t/\rho,t/\rho')$ thus approaches a finite limit for $\rho\to\infty$, given by

$$\tilde{K}(t,t')=\sqrt{t^2+t'^2}F\left(\frac{2tt'}{t^2+t'^2}\right),$$

$$F(z)=\frac{8}{\pi}\int_0^{2\pi}\frac{d\varphi}{2\pi}\sqrt{1-z\cos\varphi}. \tag{A7}$$

In the same limit we can replace the factors $[1-(t'/\rho)^2]^{-1/2}$ in Eq. (A6) by 1, and obtain the scaling equation

$$\tilde{h}(t)=\langle\tilde{K}(t,t')-\tilde{K}(0,t')\rangle_{t'}, \tag{A8}$$

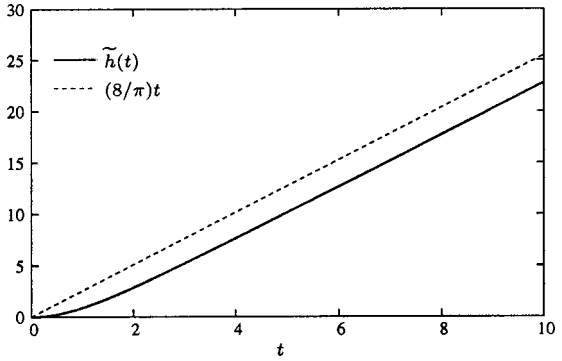

FIG. 12. Numerical solution of Eq. (A8) for the scaling function $\tilde{h}(t)$ (solid) together with the asymptotic linear behavior at large t (dashed).

where the average over t' is over the normalized probability distribution

$$\tilde{P}(t)=\frac{1}{\gamma}t\,e^{-\tilde{h}(t)},\quad \gamma=\int dt\,t\,e^{-\tilde{h}(t)} \tag{A9}$$

of the scaling variable t, now running over the range $0\ldots\infty$, since we have taken $\rho\to\infty$. A plot of the numerical solution of Eq. (A8) is shown in Fig. 12 and has the expected leading linear behavior at large t. In the high-density limit, by the same arguments as above, the normalization factor for the orientational distribution (A3) becomes $\int\widetilde{d\theta}\exp[-\tilde{h}(\rho\sin\theta)]=\gamma/\rho^2$, with γ the normalization factor defined in Eq. (A9). Thus,

$$P(\theta)=\frac{\rho^2}{\gamma}e^{-\tilde{h}(\rho\sin\theta)}. \tag{A10}$$

Inserting this into expression (A1) for the free energy and transforming everywhere from θ to t, one has

$$f=\rho(\ln\rho-1)+2\rho\ln\rho-\rho[\langle\tilde{h}(t)\rangle_t-\ln\gamma]+\frac{1}{2}\rho\langle\tilde{K}(t,t')\rangle_{t,t'}. \tag{A11}$$

From this, it follows that the osmotic pressure for large densities is simply

$$\Pi=\rho\frac{\partial f}{\partial\rho}-f=3\rho. \tag{A12}$$

It then also follows that the excess free energy $\tilde{f}$ [the last term in Eq. (A11)] is just 2ρ. This can be seen by comparing result (A12) with that obtained via a different route. Since $P(\theta)$ is determined by minimizing the free energy, one can evaluate $\Pi=\rho\,\partial f/\partial\rho-f$ by differentiating Eq. (A1), while holding $P(\theta)$ constant. Because the excess free energy is quadratic in ρ for constant $P(\theta)$, this gives $\Pi=\rho+\tilde{f}$ and therefore $\tilde{f}=2\rho$ by comparison with Eq. (A12), as claimed.

The result $\tilde{f}=2\rho$ is also useful for deriving an identity that we use in the main text to show that $\Pi=3\rho$ holds in the nematic shadow phase at the onset of the phase separation in a system with a fat-tailed length distribution with a large cutoff. The excess free energy is the last term in Eq. (A11), thus

$$\frac{1}{2}\rho\langle\tilde{K}(t,t')\rangle_{t,t'}=2\rho. \tag{A13}$$

From Eq. (A8) and $\tilde{K}(0,t')=(8/\pi)t'$, we also have

$$\langle\tilde{K}(t,t')\rangle_{t'}=\langle\tilde{K}(t,t')-\tilde{K}(0,t')\rangle_{t'}+\frac{8}{\pi}\langle t'\rangle_{t'}=\tilde{h}(t)+\frac{8}{\pi}\langle t\rangle_t. \tag{A14}$$

Inserting into Eq. (A13) we then obtain the desired identity

$$\langle\tilde{h}(t)\rangle_t+\frac{8}{\pi}\langle t\rangle_t=4. \tag{A15}$$

Notice that arguments very similar to those above apply also to *polydisperse* nematics: one again has a scaling solution $h(\theta)=\tilde{h}(t)$ for high density, in terms of the same scaling variable, and this again leads to $\Pi=3\rho$ and $\tilde{f}=2\rho$. van Roij and Mulder [22] showed this explicitly for the bidisperse case.

APPENDIX B: THE APPROXIMATION OF DOMINANCE OF THE LONG RODS

Our theory in Sec. IV for the onset of phase separation in systems with fat-tailed length distributions was based on the assumption that the nematic shadow phase is dominated by the longest rods in the system. This allowed us to replace terms that depended weakly on rod length l by their values at the cutoff l_m. We now verify that this assumption is justified in the four cases where we have used it, namely, in Eqs. (21)–(23) and (25). Let us start from the simplest of these, Eq. (21). Define the angular integral

$$A(l)=\int\widetilde{d\theta}\;e^{-(l/l_m)h(\theta)}.$$

The density distribution (20) in the nematic shadow phase is then $\rho^N(l)=\rho P^{(0)}(l)e^{lg(0)}A(l)$. The normalized nematic length distribution $P^N(l)=\rho^N(l)/\rho^N$ can be written as $P^N(l)=Q(l)A(l)/A(l_m)$, if we define

$$Q(l)=\frac{\rho}{\rho^N}P^{(0)}(l)e^{lg(0)}A(l_m).$$

Looking back at Eq. (21), the assumption of long-rod dominance amounted to replacing the weakly varying factor $A(l)/A(l_m)$ by $A(l_m)/A(l_m)=1$, effectively substituting $Q(l)$ for $P^N(l)$. To check that this is justified, we need to consider the unapproximated Equation (20), which after integration over l and division by ρ^N reads

$$\int dl\,Q(l)\frac{A(l)}{A(l_m)}=1. \tag{B1}$$

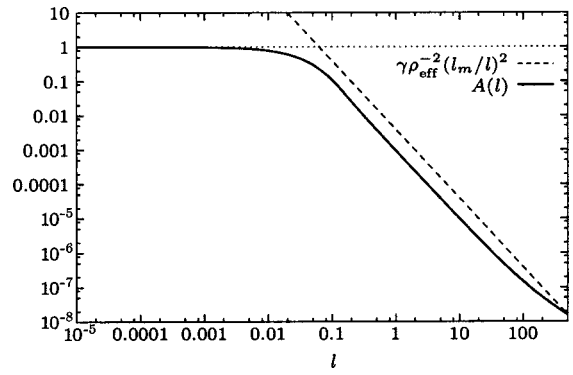

FIG. 13. Plot of $A(l)$ against l for $l_m=500$ and $\rho_{\rm eff}=6500$ ($\approx l_m \ln^2 l_m$). Notice the $\gamma\rho_{\rm eff}^{-2}(l_m/l)^2$ scaling at intermediate values of l and the quasiconstant behavior at small l. At $l\sim l_m$, corrections to the $(l_m/l)^2$ behavior are visible.

We effectively approximated this by $\int dl\, Q(l)=1$, so we need to show that the contribution from the short rods to Eq. (B1) is negligible compared to unity. We will need the l dependence of $A(l)$ to do this. Restricting the integration range to $0\ldots\pi/2$ by symmetry, using the scaling form of $h(\theta)=\tilde{h}(t)$, and transforming to the scaling variable $t=\rho_{\rm eff}\sin\theta$ gives

$$A(l)=\rho_{\rm eff}^{-2}\int_0^{\rho_{\rm eff}} dt\,\frac{t}{\sqrt{1-(t/\rho_{\rm eff})^2}}e^{-(l/l_m)\tilde{h}(t)}. \qquad \text{(B2)}$$

In the limit $l\to 0$ one has $A(l)=1$, and $A(l)$ will remain of this order while the exponential $\exp[-(l/l_m)\tilde{h}(t)]$ is close to unity even for $t=\rho_{\rm eff}$. Since $\rho_{\rm eff}$ is large and $\tilde{h}(t)$ linear in t for large arguments, this gives the criterion $(l/l_m)\rho_{\rm eff}\sim 1$ or $l\sim l_m/\rho_{\rm eff}$. Up to this value of l, we can approximate $A(l)\approx 1$. For larger l, the factor $\exp[-(l/l_m)\tilde{h}(\rho_{\rm eff})]$ is small enough for the integral to be dominated by values $t\ll\rho_{\rm eff}$, so that we can set $[1-(t/\rho_{\rm eff})^2]^{1/2}\approx 1$ and extend the upper limit of the t integral to infinity. The bulk of the integral still comes from values of $t\gg 1$, however, where $\tilde{h}(t)$ is linear, and carrying out integral (B2) with this approximation gives the scaling $A(l)\sim\rho_{\rm eff}^{-2}(l_m/l)^2$. As l increases, the range of t values contributing to the integral reduces, and eventually the quadratic behavior of $\tilde{h}(t)$ near $t=0$ leads to corrections to this scaling. Even at $l=l_m$, however, these effects are relatively small, since $\tilde{h}(t)$ is approximately linear even down to $t\approx 1$ (see Fig. 12); we therefore neglect them to a first approximation. In summary, we thus have the scaling $A(l)\sim 1$ for $l\ll l_m/\rho_{\rm eff}$, and $A(l)\sim\rho_{\rm eff}^{-2}(l_m/l)^2$ for $l\gg l_m/\rho_{\rm eff}$. A sample plot of $A(l)$ evaluated numerically, together with our approximation, is given in Fig. 13. It follows from the above results that the factor $A(l)/A(l_m)$ in Eq. (B1) is no larger than $\sim(l_m/l)^2$, even for very small l. The contribution to the l integral from rod lengths l of the order of unity is therefore bounded by $\sim\int dl\, l_m^2 l^{-2}Q(l)$. For $l=O(1)$, we can set the factor $\exp[lg(0)]$ in $Q(l)$ to 1, since $g(0)$ is small (for large l_m); the factor ρ/ρ^N is also asymptotically just an unimportant constant. The short-rod contribution to Eq. (B1) is thus of the order $\sim A(l_m)l_m^2\int dl P^{(0)}(l)l^{-2}$ or, if we extend the integral up to $l=\infty$, $A(l_m)l_m^2\langle l^{-2}\rangle$ with the average taken over the parent distribution. Now $A(l_m)\sim\rho_{\rm eff}^{-2}$ [more precisely, $A(l_m)=\gamma\rho_{\rm eff}^{-2}$; see before Eq. (A10)], so this contribution scales as $(l_m/\rho_{\rm eff})^2\sim(l_m\rho^N)^{-2}$. For the log-normal length distribution, $\rho^N\sim(\ln^2 l_m)/l_m$, and so the short-rod contribution $\sim 1/\ln^4 l_m$ to Eq. (B1) does indeed become negligible for large l_m when compared to the long-rod contribution of 1.

Next, consider the approximated osmotic pressure equation (25). We need to show that the contribution of the short rods to the l integral in Eq. (24) is negligible compared to the long-rod part, which we evaluated to be $2\rho^N$. Dividing by ρ^N to have a quantity to which the long rods contribute a value of the order of unity, and discarding factors that are constant for large l_m, we have to consider the integral

$$\int dl\, Q(l)\frac{l}{l_m}\frac{A(l)}{A(l_m)}\left\{l_m[g(0)-c_1\rho]-\frac{1}{A(l)}\int \widetilde{d\theta}\, e^{-(l/l_m)h(\theta)}h(\theta)\right\}.$$

The first term in the curly brackets is easy: the l integral is proportional to $\int dl\, Q(l)(l/l_m)[A(l)/A(l_m)]$. Comparing with the integral $\int dl\, Q(l)[A(l)/A(l_m)]$ treated above, the short-rod contribution here is suppressed by an additional factor of l/l_m, and so definitely negligible. The second term, on the other hand, is of the form

$$\int dl\, Q(l) l\frac{A(l)}{A(l_m)}\frac{A'(l)}{A(l)}=\int dl\, Q(l) l\frac{A(l)}{A(l_m)}\frac{d}{dl}\ln A(l).$$

As we saw above, $A(l)$ varies at most as a power law with l, so that $(d/dl)\ln A(l)\sim 1/l$ and we are again led back to the integral $\int dl\, Q(l)[A(l)/A(l_m)]$ for which we showed the dominance of the long rods above. [This argument applies even in the small-l range $l<l_m/\rho_{\rm eff}$, where $A(l)$ is approximately constant and $(d/dl)\ln A(l)$ therefore even smaller.]

In Eq. (18), which we approximated by Eq. (22), we have a similar l integral that turned out to scale as $1/l_m$ [see Eq. (32)]. Multiplying then by l_m to again have a long-rod contribution of the order of unity, and using $\rho l l_m=(\rho/\rho^N)(l/l_m)\rho_{\rm eff}\sim(l/l_m)\rho_{\rm eff}$, we need to consider the integral

$$\int dl\, Q(l)\frac{l}{l_m}\frac{A(l)}{A(l_m)}\int \widetilde{d\theta}\,\frac{8}{\pi}\rho_{\rm eff}\sin\theta\frac{e^{-(l/l_m)\tilde{h}(\rho_{\rm eff}\sin\theta)}}{A(l)}. \qquad \text{(B3)}$$

As before, the angular integral will be dominated (with the exception of very small lengths $l<l_m/\rho_{\rm eff}$; see below) by the range where $t=\rho_{\rm eff}\sin\theta$ is large. In this range, $\tilde{h}(t)\approx(8/\pi)t$ is linear to a good approximation, so that the angular integral can be written as

$$\int \widetilde{d\theta}\,\tilde{h}(\rho_{\rm eff}\sin\theta)\frac{e^{-(l/l_m)\tilde{h}(\rho_{\rm eff}\sin\theta)}}{A(l)}=\frac{l_m}{A(l)}.$$

The overall integral (B3) thus becomes $\int dl\ Q(l) l[A(l)/A(l_m)](d/dl)\ln A(l)$ for which the long-rod dominance has been shown already. The contribution from very small l values, $l<l_m/\rho_{\rm eff}$ needs to be treated separately. Here, we use the fact that the angular integral in Eq. (B3) can be viewed as an average of $(8/\pi)\rho_{\rm eff}\sin\theta$ over a normalized distribution, giving a result of at most $\sim\rho_{\rm eff}$. Using also that $A(l)\simeq 1$ in this regime, one needs to integrate $\rho_{\rm eff}Q(l)(l/l_m)[1/A(l_m)]$ over the range $l=0\ldots(l_m/\rho_{\rm eff})$; the integrand is bounded there by $Q(l)/A(l_m)\sim P^{(0)}(l)$ and gives a vanishing integral, since the upper limit of the integration range, $l_m/\rho_{\rm eff}=1/(\rho^N l_m)\sim 1/\ln^2 l_m$, vanishes in the limit $l_m\to\infty$.

Finally, we need to analyze Eq. (19), which we approximated by Eq. (23). Let us rewrite the rhs of Eq. (19) as

$$\frac{\rho_{\rm eff}}{A(l_m)}\int \widetilde{d\theta'}[K(\theta,\theta')-K(0,\theta')]\int dl\ Q(l)\frac{l}{l_m}e^{-(l/l_m)h(\theta')}.$$

One can view this as an average of the term in square brackets over a (unnormalized) distribution over θ'. We thus need to show that the short-rod contribution to

$$\int dl\ Q(l)\frac{l}{l_m}e^{-(l/l_m)h(\theta')} \tag{B4}$$

is negligible compared to the long-rod contribution, at least for the values of θ' that are in the bulk of this distribution (rather than the tail). When evaluating the long-rod contribution it is not *a priori* clear that one can treat the exponential factor $\exp[-(l/l_m)h(\theta')]$ as weakly varying with l. We will see below that this can nevertheless be justified, so that the long-rod contribution is simply $e^{-h(\theta')}$ as used in Eq. (23). The short-rod contribution to Eq. (B4) can be estimated by again approximating $\exp[lg(0)]\approx 1$ and bounding $\exp[-(l/l_m)h(\theta')]<1$. This yields a contribution of at most $\int dl\ P^{(0)}(l)(l/l_m)A(l_m)<\langle l\rangle A(l_m)/l_m$ with the average again taken over $P^{(0)}(l)$ and thus giving unity. This is comparable with the long-rod term $\exp[-h(\theta')]$ only for values of θ' such that $e^{-h(\theta')}\sim A(l_m)/l_m\sim 1/l_m\rho_{\rm eff}^2\sim O(l_m^{-3}\ln^{-4} l_m)$. This means that the corrections due to the short-rod integral become important only where the angular distribution has already decayed to $\sim 1/l_m^3$ (up to logarithmic terms) of its value at $\theta'=0$, i.e., far in the tails of the θ' distribution. We can now also justify neglecting the l dependence of the term $\exp[-(l/l_m)h(\theta')]$: at the onset of corrections from the short rods one has $h(\theta')\sim\ln l_m$. Up to this point, i.e., in the bulk of the distribution, the ratio $h(\theta')/l_m$ is at most $\sim(\ln l_m)/l_m$. In the overall exponential factor in Eq. (B4), $\exp\{l[g(0)-h(\theta')/l_m]\}$, this term is therefore still negligible compared to $g(0)\sim(\ln^2 l_m)/l_m$, and the resulting l dependence can be ignored.

APPENDIX C: THE DOMINANCE OF LONG RODS FOR THE SCHULZ DISTRIBUTION

In this appendix we outline briefly how, for the Schulz distribution (43), one can establish that the assumption of the long rods being dominant in the nematic shadow phase is again justified (for $z<3$). As an example we discuss Eq. (21), which is obtained from Eq. (20) if the long rods dominate.

As we saw in Appendix B, the scaling of the angular integral $A(l)=\int\widetilde{d\theta}\ e^{-(l/l_m)h(\theta)}$ is $\rho_{\rm eff}^{-2}(l_m/l)^2$ for $l>l_m/\rho_{\rm eff}$, and $A(l)\approx 1$ for smaller l. Inserting this into the nematic density distribution (20), $\rho^N(l)=\rho P^{(0)}(l)e^{lg(0)}A(l)$, using $\rho_{\rm eff}=\rho^N l_m^2$ and exploiting that ρ and ρ^N approach constant limits for $l_m\to\infty$, one has $\rho^N(l)\sim l_m^{-2}l^{z-2}e^{\delta l}$ for $l>l_m/\rho_{\rm eff}\sim 1/l_m$, and $\rho^N(l)\sim l^z e^{\delta l}$ for smaller l. We want to show again that the integral of $\rho^N(l)$ over the short rods (with lengths l of order unity) is negligible compared to the long-rod contribution [which, since $\rho^N=O(1)$, is of the order of unity]. In the short rods regime we can approximate $e^{\delta l}\simeq 1$. The integration of $\rho^N(l)$ over the range $0\ldots 1/l_m$ then gives just $\sim O(l_m^{-z-1})$ which is negligible compared to unity for $z\geqslant 0$. The contribution from the range $l>1/l_m$ can be bounded by extending the integration not just over the short rods, but in fact up to l_m, giving $\sim l_m^{-2}(l_m^{z-1}-l_m^{1-z})=(l_m^{z-3}-l_m^{-z-1})$ which is again negligible compared to unity as long as $z<3$. (For $z=1$, the integral has a logarithmic correction, giving $\sim l_m^{-2}\ln l_m$, but is still negligible.) As in the log-normal case, the integral over the nematic density distribution is therefore dominated by the longest rods, justifying Eq. (21).

[1] F.C. Bawden and N.W. Pirie, Proc. R. Soc. London **123**, 274 (1937).
[2] F.C. Bawden and N.W. Pirie, Nature (London) **141**, 513 (1938).
[3] F.C. Bawden, N.W. Pirie, J.D. Bernal, and I. Fankuchen, Nature (London) **138**, 1051 (1936).
[4] J.D. Bernal and I. Fankuchen, Nature (London) **139**, 923 (1937).
[5] J.D. Bernal and I. Fankuchen, J. Gen. Physiol. **25**, 111 (1941).
[6] L. Onsager, Ann. N.Y. Acad. Sci. **51**, 627 (1949).
[7] J. Herzfeld, A.E. Berger, and J.W. Wingate, Macromolecules **17**, 1718 (1984).
[8] S.D. Lee and R.B. Meyer, J. Chem. Phys. **84**, 3443 (1986).
[9] A. Isihara, J. Chem. Phys. **19**, 1142 (1951).
[10] T. Odijk, Macromolecules **19**, 2314 (1986).
[11] Richard F. Kayser, Jr. and Harold Raveché, Phys. Rev. A **17**, 2067 (1978).
[12] H.N.W. Lekkerkerker, P. Coulon, R. van der Haegen, and R. Deblieck, J. Chem. Phys. **80**, 3427 (1984).
[13] P.A. Buining and H.N.W. Lekkerkerker, J. Phys. Chem. **97**, 11 510 (1993).
[14] M.P.B. van Bruggen, F.M. van der Kooij, and H.N.W. Lekkerkerker, J. Phys.: Condens. Matter **8**, 9451 (1996).
[15] R.M.L. Evans, J. Chem. Phys. **114**, 1915 (2001).
[16] Zheng Yu Chen, Phys. Rev. E, **50**, 2849 (1994).
[17] T.J. Sluckin, Liq. Cryst. **6**, 111 (1989).

[18] N. Clarke, J.A. Cuesta, R. Sear, P. Sollich, and A. Speranza, J. Chem. Phys. **113**, 5817 (2000).
[19] T.M. Birshtein, B.I. Kolegov, and V.A. Pryamistsyn, Polym. Sci. U.S.S.R. **30**, 316 (1988).
[20] G.J. Vroege and H.N.W. Lekkerkerker, J. Phys. Chem. **97**, 3601 (1993).
[21] G.J. Vroege and H.N.W. Lekkerkerker, Colloids Surf., A, **130**, 405 (1997).
[22] R. van Roij and B. Mulder, J. Chem. Phys. **105**, 11 237 (1996).
[23] S. Varga and I. Szalai, Phys. Chem. Chem. Phys. **2**, 1955 (2000).
[24] K. Šolc, Macromolecules **8**, 819 (1975).
[25] K. Šolc, Macromolecules **3**, 665 (1970).
[26] A. Speranza and P. Sollich, J. Chem. Phys. **118**, 5213 (2003).
[27] A. Speranza and P. Sollich, J. Chem. Phys. **117**, 5421 (2002).
[28] E. Isaacson and H. Bishop Keller, *Analysis of Numerical Methods* (Wiley, New York, 1966).
[29] W.H. Press, S.A. Teukolsky, W.T. Vetterling, and B.P. Flannery, *Numerical Recipes in C*, 2nd ed. (Cambridge University Press, Cambridge, 1992).
[30] G.J. Vroege and H.N.W. Lekkerkerker, Rep. Prog. Phys. **55**, 1241 (1992).
[31] P.J. Flory, Proc. R. Soc. London, Ser. A **234**, 73 (1956).
[32] P.J. Flory and A. Abe, Macromolecules **11**, 1119 (1978).
[33] A. Abe and P.J. Flory, Macromolecules **11**, 1122 (1978).
[34] P. Sollich and M.E. Cates, Phys. Rev. Lett. **80**, 1365 (1998).
[35] P.B. Warren, Phys. Rev. Lett. **80**, 1369 (1998).
[36] P. Sollich, P.B. Warren, and M.E. Cates, Adv. Chem. Phys. **116**, 265 (2001).
[37] P. Sollich, J. Phys.: Condens. Matter **14**, R79 (2002).
[38] R. van Roij and B. Mulder, Europhys. Lett. **34**, 201 (1996).